Cathepsin D exacerbates SPARC-driven aggressiveness by limited proteolysis in triple-negative breast cancer

Lindsay B Alcaraz[1], Aude Mallavialle[1], Timothée David[1], Danielle Derocq[1], Frédéric Delolme[2,3], Cindy Dieryckx[2,3], Florence Boissière-Michot[4], Joëlle Simony-Lafontaine[4], Stanislas Du Manoir[1], Pitter F. Huesgen[5,6], Christopher M. Overall[5], Sophie Tartare-Deckert[7], William Jacot[1,4,8], Thierry Chardès[1], Séverine Guiu[1,8], Pascal Roger[1,9], Thomas Reinheckel[10], Catherine Moali[2,3], Emmanuelle Liaudet-Coopman[1*]

[1]IRCM, INSERM U1194, Univ Montpellier, ICM, Montpellier, France.

[2]University of Lyon, CNRS UMR5305, Tissue Biology and Therapeutic Engineering Laboratory (LBTI), F-69367 Lyon, France

[3]University of Lyon, ENS de Lyon, INSERM US8, CNRS UMS3444, SFR Biosciences, F-69366 Lyon, France

[4]Translational Research Unit, ICM, Montpellier, France.

[5]University of British Columbia, Faculty of Dentistry, Centre for Blood Research, British Columbia, V6T 1Z3, Canada.

[6]Forschungszentrum Jülich, ZEA-3 Analytics, 52428 Jülich, Germany

[7]Côte d'Azur University, Inserm, C3M, Nice, France.

[8]Department of Medical Oncology, ICM, Montpellier, France.

[9]Department of Pathology, CHU Nîmes, Nîmes, France.

[10]Institute of Molecular Medicine and Cell Research, Faculty of Medicine, Albert-Ludwigs-University Freiburg, 79104 Freiburg, Germany.

*Corresponding author: E Liaudet-Coopman, E-mail: emmanuelle.liaudet-coopman@inserm.fr

Running Tittle: Cathepsin D cleaves SPARC in the TNBC microenvironment

Keywords: matricellular protein, protease, tumor microenvironment, TNBC

Disclosure of Potential Conflicts of Interest

No potential conflicts of interest were disclosed by the other authors

ABSTRACT

Tumor-specific molecular targets and alternative therapeutic strategies for triple-negative breast cancer (TNBC) are urgently needed. The protease cathepsin D (cath-D) is a marker of poor prognosis in TNBC and a tumor-specific extracellular target for antibody-based therapy. The identification of cath-D substrates is essential for the mechanistic understanding of its role in TNBC and future therapeutic developments. Using degradomic analyses by TAILS, we discovered that the matricellular protein SPARC is a substrate of extracellular cath-D. *In vitro,* cath-D induced limited proteolysis of SPARC C-terminal extracellular Ca^{2+} binding domain at acidic pH, leading to the production of SPARC fragments (34-, 27-, 16-, 9-, and 6-kDa). Similarly, cath-D secreted by human TNBC and mouse mammary cancer cells cleaved fibroblast- and cancer-derived SPARC at the tumor pericellular pH. SPARC cleavage also occurred *in vivo* in TNBC and mouse mammary tumors. Among these fragments, the C-terminal 9-kDa SPARC fragment inhibited MDA-MB-231 TNBC cell adhesion and spreading on fibronectin, and stimulated their migration, endothelial transmigration and invasion more potently than full-length SPARC. These results highlight a novel crosstalk between proteases and matricellular proteins in the TNBC microenvironment through limited proteolysis of SPARC, and reveal that the 9-kDa C-terminal SPARC fragment is an attractive therapeutic target for TNBC.

Significance: We show that cath-D-mediated limited proteolysis of SPARC promotes its pro-tumor activity in TNBC. Our study will pave the way for the development of strategies for targeting bioactive fragments from matricellular proteins in TNBC.

INTRODUCTION

Breast cancer (BC) is one of the leading causes of death in women in developed countries. Triple-negative breast cancer (TNBC), defined by the absence of oestrogen receptor (ER), progesterone receptor (PR) and human epidermal growth factor receptor 2 (HER-2) overexpression and/or amplification, accounts for 15-20% of all BC cases (1). Chemotherapy is the primary systemic treatment, but resistance to this treatment is common (1). Thus, tumor-specific molecular targets are urgently needed to develop alternative therapeutic strategies for TNBC.

Human cathepsin D (cath-D) is a ubiquitous, lysosomal, aspartic endoproteinase that is proteolytically active at acidic pH. Cath-D expression levels in BC (2-4) and TNBC (5,6) correlate with poor prognosis. Cath-D over-production by BC and TNBC cells leads to hypersecretion of the 52-kDa cath-D precursor in the extracellular environment (6,7). Purified 52-kDa cath-D self-activates in acidic conditions, giving rise to a catalytically active 51-kDa pseudo-cath-D form that retains the 18 residues (27-44) of the pro-segment (8). Cath-D affects the tumor and its microenvironment by increasing proliferation of BC cells (7,9-12), and by stimulating mammary fibroblast outgrowth (13,14), angiogenesis (9,15), and metastasis formation (11). However, little is known about the molecular mechanisms and the substrates involved in these processes. Our recent study indicated that cath-D is a tumor-specific extracellular target in TNBC and its suitability for antibody-based therapy (16).Thus, the identification of the cath-D extracellular substrate repertoire by N-Terminal Amine Isotopic Labeling of Substrates (N-TAILS) degradomics (17) is important for the mechanistic understanding of its role in TNBC.

In a previous work using TAILS (18), we isolated the matricellular protein SPARC (Secreted Protein Acidic and Rich in Cysteine), also known as osteonectin or basement membrane 40 (BM40), as a putative cath-D substrate. SPARC is a Ca^{2+}-binding glycoprotein that regulates extracellular matrix assembly and deposition, growth factor signalling, and interactions between cells and their surrounding extracellular matrix (19-22). In cancer, SPARC is mainly secreted by the neighbouring stroma, but also by cancer cells (23-25). In different cancer types, SPARC plays an oncogenic or a tumor-suppressive role (26,27). For instance, in BC, SPARC has a pro-tumorigenic role and has been associated with worse

prognosis (24,28-33); however, other studies reported anti-tumorigenic functions (34-36). SPARC includes three different structural and functional modules: the N-terminal acidic domain, followed by the follistatin-like domain, and the C-terminal extracellular Ca^{2+} binding domain (21). Protein fragments that correspond to these SPARC domains display distinct biological functions in cell de-adhesion and spreading, motility, proliferation, invasion, and in matrix remodelling (21,22,37,38). This suggests that SPARC activity may be modulated by proteolysis, leading to the unmasking of domains with biological functions that are distinct from those described for the full-length (FL) protein.

Here, we found that in the acidic tumor microenvironment of TNBC, cath-D cleaved SPARC exclusively in its C-terminal extracellular Ca^{2+} binding domain releasing five main fragments (34-, 27-, 16-, 9-, and 6-kDa). Among these fragments, the 9-kDa C-terminal SPARC fragment (amino acids 235-303) had greater oncogenic activity than FL SPARC, highlighting the importance of limited proteolysis of matricellular proteins in the TNBC microenvironment. This knowledge might pave the way to the development of strategies to target the bioactive fragments of matricellular proteins in cancer.

RESULTS

Identification of SPARC as an extracellular protein affected by cath-D deficiency

Using the TAILS approach, we previously analysed the secretome of immortalized *Ctsd*$^{-/-}$ MEFs stably transfected with empty vector (*Ctsd*$^{-/-}$) or a human cath-D (*Ctsd*$^{-/-}$cath-D) plasmid to determine cath-D effect on extracellular protein processing (18). We noticed that the SPARC peptide LDSELTEFPLR [156-166] was 5.2-fold less abundant in the secretome of *Ctsd*$^{-/-}$cath-D MEFs than of *Ctsd*$^{-/-}$ MEFs (Fig. 1A). To determine whether SPARC is a putative cath-D substrate, we first confirmed that SPARC protein level was reduced in the *Ctsd*$^{-/-}$cath-D secretome compared with the *Ctsd*$^{-/-}$ secretome (Fig. 1B). Transcriptome analysis of *Ctsd*$^{-/-}$ and *Ctsd*$^{-/-}$cath-D MEFs, as previously published (18), showed that SPARC reduction in the *Ctsd*$^{-/-}$cath-D secretome was not due to *Sparc* gene downregulation in the presence of cath-D (Fig. 1C). These data showed that SPARC protein level in the extracellular environment is reduced in the presence of cath-D.

In vitro, cath-D cleaves SPARC extracellular Ca^{2+} binding domain at acidic pH

We investigated whether recombinant cath-D can cleave recombinant SPARC *in vitro* at acidic pH. At pH 5.9, SPARC was hydrolysed by cath-D in a time-dependent manner (Fig. 2A). Moreover, experiments in which pH was gradually reduced from 6.8 to 5.5 showed progressive limited proteolysis of SPARC at lower pH (Fig. 2B). In these two experiments, pepstatin, an aspartic protease inhibitor, inhibited SPARC cleavage by cath-D (Fig. 2A-B). By amino-terminal oriented mass spectrometry of substrates (ATOMS) analysis, we found that SPARC was hydrolysed by the 51-kDa cath-D form exclusively in its extracellular Ca^{2+} binding domain, releasing five main SPARC fragments (34-, 27, 16, 9-, and 6-kDa) at pH 5.9, detected by silver staining (Fig. 2C-E, Table 1). We detected SPARC cleavage fragments of similar size also after incubation with the fully mature 34+14-kDa cath-D form at pH 5.9 (Fig. 2C-E, Table 1). Thus, *in vitro,* cath-D triggers the limited proteolysis of SPARC exclusively in its extracellular Ca^{2+} binding domain in an acidic environment.

SPARC and cath-D expression in TNBC

To study the pathophysiological relevance of the SPARC/cath-D interplay in TNBC, we first assessed the clinical significance of *SPARC* and *CTSD* (the gene encoding cath-D) expression in a cohort of 255 patients with TNBC using an online survival analysis (39). High *CTSD* mRNA level was significantly associated with shorter recurrence-free survival (HR=1.65 for [1.08-2.53]; p=0.019) (Supplementary Fig. S1, top panel), as previously observed (16). Similarly, high *SPARC* mRNA level tended to be associated with shorter recurrence-free survival (HR=1.6 [0.91-2.79]; p=0.097) (Supplementary Fig. S1, bottom panel). We then examined SPARC and cath-D expression by immunohistochemistry (IHC) analysis in serial sections of a TNBC Tissue Micro-Array (TMA) (Fig. 3A). Cath-D was expressed mainly in cancer cells, and to a lesser extent in macrophages, fibroblasts and adipocytes in the stroma (Fig. 3A, left panel). Conversely, SPARC was expressed mainly in fibroblasts, macrophages and endothelial cells in the tumor stroma, whereas its expression level in cancer cells was variable (Fig. 3A, middle and right panels). Next, we analysed SPARC and cath-D expression and secretion in different TNBC cell lines and in human mammary fibroblasts (HMF) (Fig. 3B). Cath-D was expressed by TNBC and HMF cells (Fig. 3B, left panel), but was secreted only by TNBC cells (Fig. 3B, right panel). Conversely, SPARC was expressed and secreted by HMF, but only by two out of five TNBC cell lines, namely SUM159 and HS578T (Fig. 3B). Finally, we investigated SPARC and cath-D co-localization in a TNBC patient-derived xenograft (PDX B1995) (40) in which cath-D expression was previously demonstrated (16). Co-labelling with polyclonal anti-SPARC and monoclonal anti-cath-D antibodies (Fig. 3C) showed that SPARC (in red; panel a) partially co-localized with cath-D (in green; panel b) in the PDX B1995 microenvironment (merge; panel c). Together with previously published data on SPARC (24,28-32,41) and cath-D (2-4,6,7,9-11,13-15,42) in BC, our results strongly suggest that it is important to investigate the relationship between SPARC and cath-D that are both co-secreted in the TNBC microenvironment.

At acidic pH, cath-D secreted by TNBC and mouse mammary cancer cells cleaves fibroblast- and cancer-derived SPARC in its extracellular Ca^{2+} binding domain

As the tumor extracellular environment is acidic (43), we then asked whether cath-D can degrade SPARC in the extracellular medium of TNBC cells at low pH. First, we used conditioned medium from cath-D-secreting TNBC MDA-MB-231 cells co-cultured with SPARC-secreting HMFs for 24h (Supplementary Fig. S2). SPARC was hydrolysed in a time-dependent manner in the conditioned medium at pH 5.5 (Fig. 4A). By western blot analysis, we detected mainly the 34-kDa and 27-kDa SPARC fragments, and to a lesser extent, the 16-kDa fragment (Fig. 4A). Pepstatin A inhibited SPARC cleavage, confirming the involvement of secreted aspartic protease proteolytic activity (Fig. 4A). Moreover, TAILS analysis of the secretome in conditioned medium of co-cultured MDA-MB-231/HMF cells at pH 5.5 showed the presence of the five main SPARC fragments (34, 27-, 16-, 9-, and 6-kDa) only in the absence of pepstatin A (Table 1). We then assessed SPARC hydrolysis at different pH (6.8 to 5.5), and found that in the MDA-MB-231/HMF conditioned medium, SPARC was significantly degraded up to pH 6.2 (Fig. 4B), similarly to the results obtained with recombinant proteins (Fig. 2B). In addition, we observed SPARC limited proteolysis also in conditioned medium of TNBC HS578T (Fig. 4C) and TNBC SUM159 cells (Fig. 4D), which secrete both proteins, at pH 5.5. Finally, we did not observe SPARC cleavage at pH 5.5 in conditioned medium from HMFs co-cultured with MDA-MB-231 cells in which *CTSD* was silenced by RNA interference, indicating that cath-D was responsible for SPARC proteolysis in acidic conditions (Fig. 4E). We confirmed cath-D direct involvement in SPARC processing also by using a mammary cancer cell line derived from tamoxifen-inducible $Cre^{ERT2,}$ $Ctsd^{fl/fl}$ mice (44) crossed with the transgenic MMTV-PyMT mouse model of metastatic BC (45) (Fig. 4F). In the absence of hydroxytamoxifen (OH-Tam), both cath-D and SPARC were secreted by these cells, whereas cath-D expression and secretion were abrogated by incubation with OH-Tam (Supplementary Fig. S3). SPARC was hydrolysed in the conditioned medium from this mouse mammary cancer cell line at pH 5.5 only in the absence of OH-Tam when cath-D was secreted (Fig. 4F). These findings demonstrate that cath-D secreted by TNBC and mouse mammary tumor cells cleaves SPARC in its extracellular Ca^{2+} binding domain at the acidic pH found in the tumor microenvironment.

SPARC is cleaved *in vivo* in TNBC and mouse mammary tumors

To validate cath-D-dependent SPARC cleavage *in vivo*, we first analysed FL SPARC protein level and its cleaved fragments in whole cytosols of mammary tumors from MMTV-PyMT cath-D knock-out mice (Fig. 5A). As expected, cath-D was expressed in the cytosol of mammary tumors from MMTV-PyMT, *Ctsd*$^{+/+}$ mice, but not from MMTV-PyMT, *Ctsd*$^{-/-}$ mice (Fig. 5A, left panel). In two of the three tumors from MMTV-PyMT, *Ctsd*$^{-/-}$ mice, SPARC expression level was much higher than in the three tumors from MMTV-PyMT, *Ctsd*$^{+/+}$ mice (Fig. 5A, left panel). Unexpectedly, we could not detect any SPARC cleavage fragment in this transgenic mouse model, certainly due to further SPARC proteolysis *in vivo* by other proteinases. Nevertheless, SPARC reduction occurred through post-translational mechanisms because *SPARC* mRNA level was not significantly different in the corresponding MMTV-PyMT, *Ctsd*$^{+/+}$ and MMTV-PyMT, *Ctsd*$^{-/-}$ tumors (Fig. 5A, right panel). We then evaluated the presence of FL SPARC and its cleaved fragments in the whole cytosols from two TNBC PDXs that express cath-D at high and low level, respectively (Fig. 5B, top panel). We detected FL SPARC and its 34-kDa cleaved fragment in PDX B3977 (high cath-D expression), but only FL SPARC in PDX B1995 (low cath-D expression) (Fig. 5B, bottom panel). Finally, we analysed the level of FL SPARC and its cleaved fragments in whole cytosols from two TNBC clinical samples with different cath-D expression levels (Fig. 5C, top panel). The level of FL SPARC was lower in cytosol C1 (TNBC with high cath-D expression) than in cytosol C2 (TNBC with low cath-D expression) (Fig. 5C, bottom panel). Moreover, we detected the 27-kDa cleaved SPARC fragment only in cytosol C1 (high cath-D expression) (Fig. 5C, bottom panel). Overall, these results strongly suggest that SPARC cleavage in its extracellular Ca^{2+} binding domain may occur *in vivo* in mammary cancers in the presence of cath-D, although other proteinases may also be involved.

Cath-D-induced SPARC fragments inhibit TNBC cell adhesion and spreading, and promote their motility, endothelial transmigration and invasion

Previous studies reported that FL SPARC and particularly its C-terminal extracellular Ca^{2+} binding domain can modulate adhesion, spreading, motility, endothelial transmigration, and invasion of cancer

and stromal cells (22,23,30,46-48). Therefore, we compared the effect of the cath-D-induced SPARC fragments (mixture of 34+27+16+9+ 6-kDa fragments) (Supplementary Fig. S4) and of FL recombinant SPARC (42-kDa) in MDA-MB-231 cells. Soluble FL SPARC significantly inhibited MDA-MB-231 cell adhesion on fibronectin in a dose-dependent manner (Supplementary Fig. S5). After incubation with FL SPARC (final concentration of 10 µg/ml, 240 nM), as previously described (23,46), MDA-MB-231 cell adhesion on fibronectin was reduced by 1.3-fold compared with control (CTRL; untreated) (Fig. 6A; *P<0.001).* Moreover, FL SPARC inhibition of cell adhesion was similar in Luc- and cath-D-silenced MDA-MB-231 cells, indicating an autonomous effect of SPARC on cell adhesion (Supplementary Fig. S6). Incubation of MDA-MB-231 cells with cath-D-induced SPARC fragments (cleaved SPARC) also significantly decreased cell adhesion by 1.7-fold compared with control (CTRL) (Fig. 6A; *P<0.001)* and by 1.3-fold compared with FL SPARC (Fig. 6A; *P<0.001).* We also monitored the effects of FL and cleaved SPARC on MDA-MB-231 cell spreading on fibronectin by staining F-actin filaments with phalloidin (Supplementary Fig. S7A). Both FL SPARC and SPARC cleaved fragments led to a decrease of the cell surface contact area on fibronectin through a peripheral rearrangement of F-actin. Specifically, bundling of actin stress fibres was disrupted and actin microfilaments were redistributed in a peripheral web (Supplementary Fig. S7A). This suggests a transition to an intermediate state of adhesiveness, previously described for FL SPARC (49), that may favour cell migration and invasion (50). Incubation with FL and cleaved SPARC fragments decreased the percentage of spread cells by 2.1-fold and 3.8-fold, respectively, compared with control (Supplementary Fig. S7B; *P<0.001*). This inhibition was significantly higher (1.8-fold) with cleaved SPARC than FL SPARC (Supplementary Fig. S7B; *P<0.05*). Then, cell motility analysis in Boyden chambers showed quite high basal motility of MDA-MB-231 cells, as expected for mesenchymal cells (e.g. 49% of cells passed through the fibronectin-coated filters) (Fig. 6B). Incubation with FL and cleaved SPARC increased MDA-MB-231 cell motility by 1.5-fold and 1.9-fold, respectively, compared with control (Fig. 6B; *P<0.01* and *P<0.001).* Moreover, the effect of cleaved SPARC on cell motility was 1.3-fold higher than that of FL SPARC (Fig. 6B; *P<0.05*). In the endothelial transmigration assay, FL and cleaved SPARC fragments stimulated MDA-MB-231 migration through primary human umbilical vein endothelial cells (HUVECs) by 1.4-fold and 1.7-fold, respectively, compared with

control (Fig. 6C; *P<0.01* and *P<0.001*). The effect of cleaved SPARC was 1.2-fold higher than that of FL SPARC (Fig. 6C; *P<0.05*). Finally, both FL and cleaved SPARC fragments increased MDA-MB-231 cell invasion through Matrigel-coated filters in Boyden chambers by 2-fold and 3-fold, respectively, compared with control (Fig. 6D; *P<0.001).* The effect of cleaved SPARC was 1.5-fold higher than that of FL SPARC (Fig. 6D; *P<0.001).* Altogether, these results indicate that FL SPARC inhibits MDA-MB-231 cell adhesion and spreading, and promotes MDA-MB-231 cell motility, endothelial transmigration, and invasion. These effects were increased by incubation with cath-D-induced SPARC fragments, suggesting that in the TNBC microenvironment, cath-D amplifies SPARC pro-tumor activity through proteolysis of its extracellular Ca^{2+} binding domain.

The 9-kDa C-terminal SPARC fragment inhibits TNBC cell adhesion and spreading, and promotes their motility, endothelial transmigration, and invasion

To identify the SPARC domain(s) involved in these functions, we produced FL SPARC and its various cleaved fragments in mammalian cells and purified them, as previously described (51,52) (Fig. 7A, Supplementary Table S1). We first determined which SPARC fragment(s) were involved in the reduction of cell adhesion by incubating MDA-MB-231 cells with equimolar amounts of FL protein and each fragment (Fig. 7B). As before (Fig. 6A), purified FL SPARC (42-kDa) reduced MDA-MB-231 cell adhesion by 1.4-fold compared with control (Fig. 7B; *P<0.001*). However, among the C-terminal SPARC fragments, only the 9-kDa fragment (amino acids 235-303) significantly decreased MDA-MB-231 cell adhesion by 2-fold compared with control (Fig. 7B; *P<0.001*), and by 1.4-fold compared with FL SPARC (Fig. 7B; *P<0.001*). The 9-kDa C-terminal SPARC fragment (amino acids 235-303) contains the two Ca^{2+} binding sequences of the two EF-hand domains (Supplementary Fig. S8), that are involved in focal adhesion disassembly, and are crucial for SPARC-mediated inhibition of adhesion (46,53). The 16-kDa C-terminal SPARC fragment (amino acids 179-303) reduced cell adhesion by 1.2-fold (not significant) (Fig. 7B; Supplementary Fig. S8), and the 6-kDa SPARC fragment (amino acids 258-303) had no effect (Fig. 7B; Supplementary Fig. S8). Therefore, among the five cath-D-induced SPARC fragments (Fig. 2E), only the C-terminal 9-kDa fragment could inhibit cell adhesion and more potently than FL SPARC.

Based on these results, we compared the effects on MDA-MB-231 cell adhesion, spreading, motility, endothelial transmigration and invasion of the 9-kDa C-terminal SPARC fragment, FL SPARC, and the mixture of cath-D cleaved SPARC fragments (34-, 27-, 16-, 9-, and 6-kDa) (Fig. 8, Supplementary Fig. S9, Supplementary Fig. S10). Incubation with the 9-kDa C-terminal SPARC fragment significantly decreased cell adhesion (Fig. 8A, $P<0.001$) and spreading (Supplementary Fig. S10, $P<0.001$) by 2.1-fold, and 8.4-fold, respectively, compared with control, and significantly increased cell motility by 1.6-fold (Fig. 8B; $P<0.001$), endothelial transmigration by 2.1-fold (Fig. 8C; $P<0.001$), and cell invasion by 1.7-fold (Fig. 8D; $P<0.001$) compared with control. Moreover, the 9-kDa SPARC fragment seemed to induce a transition to an intermediate adhesive state highlighted by the loss of actin-containing stress fibres (Supplementary Fig. S10A). Conversely, we did not observe any significant difference between the 9-kDa C-terminal SPARC and the cath-D-induced SPARC fragments (Fig. 8 and Supplementary Fig. S10).

DISCUSSION

This study shows that cath-D secreted by TNBC cells triggers fibroblast- and cancer-derived SPARC cleavage at the acidic pH of the tumor microenvironment, leading to the production of the bioactive 9-kDa C-terminal SPARC fragment that inhibits cancer cell adhesion and spreading, and stimulates their migration, endothelial transmigration and invasion (Fig. 9). The TAILS analysis of the secretomes of conditioned medium from co-cultured TNBC cells and HMFs revealed that five main SPARC fragments (34-, 27-, 16-, 9-, and 6-kDa) are released in the extracellular environment in a cath-D-dependent manner. Our previous TAILS study showed that cystatin C is a substrate of extracellular cath-D and it is completely degraded by multiple cleavage, highlighting the complexity of the proteolytic cascades that operate in the tumor microenvironment (18). Here, we demonstrate that cath-D triggers also the limited proteolysis of the matricellular protein SPARC in an acidic environment to favour TNBC invasion.

Our recent study indicated that extracellular cath-D is a therapeutic target for immunotherapy and a biomarker in TNBC (16). Moreover, Huang *et al* found that cath-D was overexpressed in 71.5% of the 504 TNBC samples analysed and proposed a prognostic model for TNBC outcome based on node status, cath-D expression and Ki67 index (5). More recently, it was found that co-expression of cath-D and androgen receptor defines a TNBC subgroup with poorer overall survival (6). SPARC protein and mRNA are also overexpressed in TNBC (31,33,54), and this has been associated with poor prognosis in patients with TNBC (30,31,33). Here, we showed that high mRNA expression of *CTSD* and *SPARC* tended to be associated with shorter recurrence-free survival in a cohort of 255 patients with TNBC using an on line survival tool (39). Moreover, in a TNBC TMA, we found that cath-D was mainly expressed by cancer cells and some stromal cells, as shown previously (16). Conversely, SPARC was mainly expressed in mesenchymal cells, while its expression level in tumor cells was variable, as previously described (24,25). *In cellulo,* cath-D was secreted by TNBC cells and SPARC by human breast fibroblasts and some TNBC cell lines, as previously described (6,35,41). Importantly, cath-D and SPARC were co-localized in the microenvironment of TNBC PDX. Overall, these data prompted us to study the interplay between cath-D and SPARC in the TNBC microenvironment.

We then demonstrated that cath-D cleaves SPARC *in vitro* in an acidic environment exclusively in its extracellular Ca^{2+} binding domain, specifically releasing five main SPARC fragments (34-, 27-, 16-, 9-, and 6-kDa). The main peptide bonds cleaved by cath-D at low pH are Phe-Phe, Leu-Tyr, Tyr-Leu, and Phe-Tyr (55) that correspond relatively well to the cleavage sites identified in this study. Interestingly, other cleavage sites were also detected, such as Leu-Val, Leu-Asp/Glu or Gln-Phe, Gly-Tyr and Ala-Pro, which confirms the preference of cath-D for cleavage sites with at least one hydrophobic residue in P1 or P1'. SPARC biological activity can be modulated by limited proteolysis, leading to the unmasking of distinct or amplified biological functions compared with those of the FL protein (48,56). For instance, matrix metalloproteinases (MMP-1, -2, -3, -9 and -13) cleave SPARC *in vitro* in its N-terminal acid domain and in its extracellular Ca^{2+} binding domain, releasing fragments with higher affinity for collagens that modulate cell-cell and cell-matrix extracellular interactions in the tumor microenvironment (57). In addition, MMP-3-mediated SPARC cleavage *in vitro* produces fragments that affect angiogenesis (58). More recently, cleavage of SPARC extracellular Ca^{2+} binding domain by MMP-8 and MMP-13 has been detected in the serum of patients with lung cancer, indicating their presence also *in vivo* (59). Similarly, the cysteine cathepsin K (cath-K) also cleaves SPARC *in vitro* and *in vivo* in its N-terminal acid domain, and in its extracellular Ca^{2+} binding domain in prostate cancer bone metastases, releasing a 10-kDa C-terminal fragment with unknown biological activity (60). It is striking that the 9-kDa SPARC fragment generated by cath-D in our study is within the 10-kDa SPARC fragment generated by cath-K (60).

We then demonstrated that at acidic pH, cath-D present in conditioned medium from cath-D-secreting MDA-MB-231 TNBC cells co-cultured with SPARC-secreting HMFs (or from HS578T and SUM159 TNBC cells that secrete both factors) induces limited proteolysis of SPARC, leading to the production of SPARC fragments with the same molecular weight (34-, 27-, and 16-kDa) detected with the recombinant proteins. By western blot analysis, we could not detect the 9-kDa and 6-kDa SPARC fragments, whereas we identified all five SPARC main fragments (34-, 27-, 16-, 9- and 6- kDa) in the TAILS analysis of the secretomes of MDA-MB-231/HMF co-cultures. Moreover, in breast cancers of transgenic mice, in TNBC PDXs and in two clinical TNBC samples that express high or low cath-D levels, we found that cath-D expression was inversely correlated with SPARC levels, and detected the

SPARC fragments of 34-kDa and 27-kDa only in samples that strongly express cath-D. Altogether, our data strongly suggest that cath-D cleaves SPARC in its extracellular Ca^{2+} binding domain *in vitro*, in the secretome of TNBC cell lines, and *in vivo* in TNBC. Importantly, SPARC peptides corresponding to the 9-kDa (236-256), 6-kDa (258-268), 16-kDa (179-191) et 27-kDa (207-218) SPARC fragments have been found in BC tumors by using an on line proteomic database (https://cptac-data-portal.georgetown.edu/) (61). To date, only one study on cath-K in prostate cancer (60) validated *in vitro, in cellulo* and *in vivo* SPARC cleavage events by proteases in cancer. In addition, to our knowledge, no study has established yet a direct link between a SPARC fragment generated by a protease activity and its biological function in TNBC.

SPARC plays multiple contextual functions depending on the cancer type and stage, and its precise role(s) in TNBC remains to be studied. FL SPARC stimulates migration and invasion of TNBC cells (62), and promotes MMP-2 activation in TNBC cells, thereby contributing to the proteolytic cascades associated with tumor invasion (41). In addition, FL SPARC stimulates tumor growth and lung colonization by murine TNBC 4T1 and LM3 cells implanted in syngeneic mice by promoting cell cycling and expansion of myeloid-derived suppressor cells (MDSCs) (32). Conversely, FL SPARC transfected in high-grade isogenic BC cells reduces tumor rate, and favours epithelial-to-mesenchymal transition and the formation of a highly immunosuppressive microenvironment composed of immune cells, such as MDSCs (30). However, the oncogenic roles of SPARC fragments generated by proteolysis in the tumor microenvironment of TNBC were not known. Here, we demonstrated that the 9-kDa C-terminal fragment of SPARC released by cath-D has greater oncogenic activity than native SPARC, showing a new crosstalk between proteases and matricellular proteins in the TNBC stroma. The 9-kDa C-terminal fragment is located in the extracellular Ca^{2+} binding domain of SPARC. The crystal structure of this SPARC domain (Protein Data Bank DOI: 10.2210/pdb2V53/pdb) showed a canonical pair of EF-hand calcium binding sites that are essential for stabilizing Ca^{2+} binding (63). We found that the 9-kDa C-terminal fragment of SPARC is an important regulator of MDA-MB-231 TNBC cell adhesion, spreading, migration, endothelial transmigration and invasion. Specifically, it inhibited cell adhesion and spreading, and induced redistribution of actin microfilaments at the periphery of TNBC cells associated with cell rounding. A previous work showed that FL SPARC inhibits endothelial cell

spreading and induces endothelial cell rounding by affecting the early stages of the counter-adhesive process through the loss of vinculin-containing focal adhesion plaques and the concomitant reorganization of actin-containing stress fibres (46). This might correspond to an intermediate adhesive state that was previously observed in endothelial cells incubated with FL SPARC (38), and in some cancer types, such as gliomas (64), and that promotes cell motility and invasion (50).

Both amino- and carboxyl-terminal (EF-hand) domains of SPARC bind to Ca^{2+} that is required for maintenance of its native structure (53). In the EF-hand motif, two helices (E and F) flank a loop of 12 amino acids in which the Ca^{2+} ion is coordinated in a pentagonal bipyramidal arrangement (65). Moreover, FL SPARC binding to the extracellular matrix is Ca^{2+}-dependent (53). Interestingly, synthetic small peptides (^{272}TCDLDNDKYIALDEWAGCFG^{291}) with sequences derived from SPARC C-terminal extracellular Ca^{2+} binding domain (EF hand-2) inhibit adhesion and spreading of endothelial cells and fibroblasts (46,49,66). In our experimental model, it seems unlikely that only the EF hand-2 (aa 262-294) domain is involved in inhibiting MDA-MB-231 cell adhesion to fibronectin. Indeed, the 6-kDa SPARC fragment (amino acids 258-303) that contains only the EF hand-2 domain did not inhibit MDA-MB-231 cell adhesion, unlike the 9-kDa SPARC fragment (amino acids 235-303) that contains the residues coordinating Ca^{2+} in both EF-hands. This suggests that the two Ca^{2+}-binding domains are involved in this effect. However, inhibition of cell adhesion by the 16-kDa SPARC fragment (amino acids 179-303) that also contains both EF-hand domains was less important compared with the 9-kDa SPARC fragment. This suggests that the additional N-terminal sequences may alter the EF-hand domain conformation, or may interfere with Ca^{2+} binding or with the interaction with fibronectin or a TNBC cell surface receptor. It also suggests that the three-dimensional conformation of the N-terminal sequences of the 16-kDa fragment is different from that of FL SPARC, which significantly inhibited MDA-MB-231 cell adhesion. It remains to be determined whether the 9-kDa C-terminal fragment of SPARC acts directly through a specific receptor, such $\alpha5\beta1$ integrin, as described for FL SPARC (22), or by blocking adhesive interactions.

In addition, we demonstrated that FL SPARC (and more strongly the 9-kDa C-terminal fragment) promoted endothelial transmigration of TNBC cells, an essential step for extravasation and metastasis, as previously shown in melanoma (23). It was previously reported that the C-terminal extracellular Ca^{2+}

module of SPARC, a domain implicated in binding to endothelial cells (67) and to vascular cell adhesion molecule 1 (VCAM1) (68), is needed to enhance endothelial transmigration of melanoma cells *via* VCAM1 signalling (23). These findings suggest a role for the 9-kDa C-terminal SPARC fragment in vascular permeability, extravasation and metastasis formation *in vivo*.

Our current results indicate that cath-D secreted by TNBC cells is part of the proteolytic network in the TNBC acidic microenvironment that generates a bioactive 9-kDa C-terminal fragment of the matricellular protein SPARC with enhanced oncogenic activity. We dissected the molecular mechanisms that link SPARC limited cleavage by cath-D in TNBC microenvironment to the amplified oncogenic activity of a 9-kDa C-terminal fragment of SPARC, highlighting a novel paradigm of alteration of the extracellular milieu of TNBC by proteolysis. Overall, these results indicate that the 9-kDa C-terminal SPARC fragment is an attractive target for cancer therapies in TNBC, and open the way for developing novel targeted therapies against bioactive fragments from matricellular proteins, for both restructuring the surrounding microenvironment and reducing tumorigenesis (69).

MATERIALS AND METHODS

Additional Materials and Methods are in Supplementary files.

Antibodies

The rabbit polyclonal anti-SPARC (15274-1-AP) was purchased from Proteintech. The mouse monoclonal anti-human SPARC antibodies (clone AON-5031, sc-73472), the rabbit polyclonal anti-human cath-D antibody (H-75, sc-10725), and the mouse monoclonal anti-human cath-D (clone C-5, sc-377124) were purchased from Santa Cruz Biotechnology. The mouse monoclonal anti-human cath-D antibody (clone 49, #610801) was purchased from BD Transduction Laboratories™, and the goat polyclonal anti-mouse cath-D (AF1029) from R&D systems. The anti-human cath-D antibodies M1G8 and D7E3 were previously described (13). The mouse monoclonal anti-tubulin antibody (clone 236-10501, #A11126) was from ThermoFisher Scientific, the mouse monoclonal anti-Myc tag (clone 9B11) from Ozyme, and the rabbit polyclonal anti-β actin antibody (#A2066) from Sigma-Aldrich. The horse anti-mouse immunoglobulin G (IgG)-horseradish peroxidase secondary (#7076), and goat anti-rabbit IgG-HRP secondary antibodies (#7074S) were purchased from Cell Signaling Technology. The donkey anti-goat HRP conjugated (FT-1I7890) antibody was from Interchim. The Alexa Fluor 488-conjugated anti-rabbit IgG (#Ab150077) was purchased from Abcam, and the Cy3-conjugated anti-mouse IgG (#SA00009.1) from Proteintech. Hoechst 33342 (#FP-BB1340) was from Interchim FluoProbes.

Cell lines, cell lysis, ELISA, and western blotting

Immortalized cath-D-deficient MEFs were provided by C. Peters (University of Freiburg, Freiburg, Germany), and HUVECs by M. Villalba (IRMB, Montpellier). Immortalized cath-D-deficient MEFs stably transfected with empty vector (*Ctsd*$^{-/-}$) or the cath-D expression plasmid encoding human pre-pro-cathepsin D (*Ctsd*$^{-/-}$cath-D) were previously described (14). HMFs were provided by J. Loncarek and J. Piette (CRCL Val d'Aurelle-Paul Lamarque, Montpellier, France) (14). The MDA-MB-231 cell line was previously described (11). The Hs578T, MDA-MB-453 and MDA-MB-468 breast cancer cell lines were obtained from SIRIC Montpellier Cancer. The SUM159 breast cancer cell line was obtained from

Asterand (Bioscience, UK). The HEK-293 cell line was kindly provided by A. Maraver (IRCM, Montpellier). Cell lines were cultured in DMEM with 10% foetal calf serum (FCS, GibcoBRL) except the SUM159 cell line that was cultured in RPMI with 10% FCS. Primary murine breast cancer cells were generated from end-stage tumors of Cre^{ERT2}, *Ctsd*$^{fl/fl}$; MMTV-PyMT mice as described previously (70). All animal procedures were approved by the legal authorities and ethics committee at the regional council Freiburg (registration numbers G14/18 and G18/38) and were performed in accordance with the German law for animal welfare. PyMT cells were cultured in DMEM/F12 medium supplemented with 10% FCS, 2 mM L-glutamine, and 1% Penicillin-Streptomycin at 37 °C with 5% CO_2. 3 µM 4-hydroxytamoxifen (OH-Tam, Sigma Aldrich) was added to induce Cre-mediated recombination in the mouse *Ctsd* gene resulting in a premature stop codon. Cell lysates were harvested in lysis buffer (50 mM HEPES [pH 7.5], 150 mM NaCl, 10% glycerol, 1% Triton X-100, 1.5 mM $MgCl_2$, 1 mM EGTA) supplemented with cOmplete™ protease and phosphatase inhibitor Cocktail (Roche, Switzerland) at 4°C for 20 min, and centrifuged at 13 000 x g at 4°C for 10 min. Protein concentration was determined using the DC protein assay (Bio-Rad). Cath-D was quantified in TNBC and PDX cytosols by sandwich ELISA, after coating with the D7E3 antibody (200 ng/well in PBS) and with the HRP-conjugated M1G8 antibody (1/80), and using recombinant cath-D (1.25-15 ng/ml), as previously described (16). TNBC cytosols were previously prepared and frozen (71). For western blotting, proteins were separated on 13.5% SDS PAGE and analysed by immunoblotting.

SPARC cleavage by cath-D *in vitro* and *in cellulo*

Recombinant 52-kDa pro-cath-D (4 µM; R&D Systems) was self-activated to 51-kDa pseudo-cath-D in 0.1 M Na-acetate buffer (pH 3.5), 0.2 M NaCl at 37°C for 15 min, as previously described (18). Recombinant SPARC (1 µM; R&D Systems) was incubated with self-activated pseudo-cath-D (5 nM) at 37°C at different pH values in cleavage buffer [34 mM Britton-Robinson buffer in the presence of phosphatidylcholine (0.12 mM; Sigma-Aldrich) and cardiolipin (0.05 mM; Sigma-Aldrich) with or without pepstatin A (2 µM; Sigma-Aldrich]. Cleaved SPARC peptides were separated by 13.5% or 17% SDS PAGE and analysed by immunoblotting or silver staining (GE Healthcare Life Sciences), respectively. For *in cellulo* SPARC cleavage, 200, 000 MDA-MB-231 cells were plated with 100 000

HMF cells in T25 cell culture flasks. After 24 h, culture medium was changed. Conditioned medium from co-cultured MDA-MB-231 cells and HMF was obtained by adding DMEM without sodium bicarbonate buffered with 50 mM HEPES buffer (pH 7.5) and without FCS for 24h. The 24h conditioned medium was then incubated, with or without pepstatin A (12.5 µM), at 37°C in cleavage buffer. Then, proteins in medium (40 µl) were separated by 13.5% SDS-PAGE and analysed by immunoblotting. In other *in cellulo* SPARC cleavage, 200, 000 Hs578T, SUM159 or PyMT cells were incubated in DMEM without sodium bicarbonate buffered with 50 mM HEPES buffer (pH 7.5) and without FCS for 24h, and the conditioned medium was analysed as described above.

Identification of cath-D-generated fragments by ATOMS

Recombinant SPARC (4 µM, 6 µg) was incubated with self-activated 51-kDa or mature 34+14-kDa cath-D (200 nM) in 100 mM Na-acetate buffer (pH 5.9)/0.2 M NaCl with or without pepstatin A (200 µM; Sigma-Aldrich) in the presence of phosphatidylcholine (0.12 mM; Sigma-Aldrich) and cardiolipin (0.05 mM; Sigma-Aldrich) at 37°C for 15 min. SPARC cleavage was analysed by 13.5% SDS PAGE and silver staining (GE Healthcare Life Sciences). The corresponding samples with/without pepstatin A (5 µg) were then processed for iTRAQ-ATOMS, as previously described (72). Briefly, samples were denatured in 2.5 M guanidine hydrochloride and 0.25 M HEPES pH 8.0 at 65 °C for 15 min, reduced with 1 mM TCEP at 65 °C for 45 min, and alkylated with iodoacetamide at room temperature in the dark for 30 min. After iTRAQ labelling in DMSO, the two samples with/without pepstatin A were mixed and precipitated with eight volumes of freezer-cold acetone and one volume of freezer-cold methanol. The pellet was washed extensively with cold methanol, dried and resuspended in 5 µl of 50 mM NaOH. The pH was adjusted to 8 with 1.8 M HEPES pH 8.0, and the sample was digested at 37 °C with sequencing-grade trypsin (Promega; 1:50 protease:protein w/w ratio) or at 25°C with Glu-C (Promega; 1:20 protease:protein w/w ratio) overnight. After desalting on a C18 column (Pierce), the sample was analysed by LC-MS/MS on a Q-Exactive HF mass spectrometer operated with the Xcalibur software (version 4.0) and equipped with a RSLC Ultimate 3000 nanoLC system (Thermo Scientific), as previously described (73). Data files were analysed with Proteome Discover 1.4 using the MASCOT (2.2 version) algorithm against the human protein database (SwissProt release 2017-01, 40500 entries

including reverse decoy database). Precursor mass tolerance was set at 10 ppm and fragment mass tolerance was set at 0.02 Da, and up to 2 missed cleavages were allowed. Oxidation (M), Deamidation (NQ), acetylation (Protein N-terminus), and iTRAQ 8Plex (N-term, K) were set as variable modifications, and carbamidomethylation (C) as fixed modification. Peptides and proteins were filtered using Percolator and a false discovery rate (FDR) of 1%. Peptides with N-terminal iTRAQ labelling were manually validated. Quantification was performed with the Reporter Ions Quantifier node. The peak integration was set to the Most Confidence Centroid with 20 ppm Integration Mass Tolerance on the reporter ions. The cath-D without pepstatin A/cath-D with pepstatin A ratios were calculated and ratios showing at least a two-fold change are conserved in Table 1 except for peptides corresponding to the mature N-Terminus.

Secretome preparation

Secretomes from *Ctsd*$^{-/-}$ and *Ctsd*$^{-/-}$cath-D cells were prepared as previously described (18). Briefly, cells were washed extensively with phenol red-free, serum-free medium to remove serum proteins and grown overnight in phenol red-free, serum-free medium. Conditioned medium was immediately incubated with protease inhibitors (1 mM EDTA, protease inhibitor cocktail (Complete; Roche Applied Science)), clarified by centrifugation (500 g for 5 min; 8,000 g for 30 min) and filtered (0.45 µM). Proteins present in conditioned medium in 50 mM HEPES (pH 7.5) were then concentrated to 2 mg/ml through Amicon filters (3 kDa cut-off, Millipore). To prepare secretomes from MDA-MB-231/HMF co-cultures, cells (ratio 1:5, respectively) were plated in 150 mm Petri dishes in DMEM with 10% FCS. At a 90% confluence, MDA-MB-231/HMF cells were washed extensively as described above. The 24h-conditioned medium in 50 mM HEPES (pH 7.5) was then concentrated to 0.2 mg/ml through Amicon filters (3 kDa cut-off, Millipore), and incubated in cleavage buffer with or without pepstatin A (12.5 µM) at pH 5.5 and at 37° for 60 min. Samples were concentrated by TCA/acetone precipitation (73).

Mass spectrometry analysis of protein N-termini in cell culture samples (TAILS)

Enrichment of N-terminal peptides by TAILS (42) by isotopic labelling of proteins with iTRAQ reagents (17) was previously described for *Ctsd*$^{-/-}$ and *Ctsd*$^{-/-}$cath-D (18). Briefly, peptides were pre-fractionated

by strong cation exchange chromatography and analysed by LC-MS/MS (QSTAR XL, Applied Biosystems). Peptides were identified at the 95% confidence level from the human UniProtKB/Swissprot protein database using two search engines, MASCOT v2.3 (Matrix Science) and X!TANDEM (74), in conjunction with PeptideProphet as implemented in the Trans Proteomic Pipeline v4.3. Search parameters were: Semi-ArgC peptides with up to two missed cleavages, 0.4 Da precursor ion mass tolerance, 0.4 Da fragment ion mass tolerance, carboxyamidomethylation of cysteine residues, and iTRAQ labelling of lysine e-amines as fixed modifications, and peptide N-terminal iTRAQ labelling, peptide N-terminal acetylation and Met oxidation as variable modifications. Results from both searches were combined using an in-house software script (75). Peptides needed to have an Arg residue at their C-terminus and an iTRAQ reporter ion intensity of >30 in at least one of the compared channels. N-terminal peptides with significant changes between conditions were identified by calculating the log2 of the intensity ratios, correcting the mean of all ratios, and applying a 3-fold change cut-off (mean-corrected log2>1.58 or <-1.58). The abundance of N-terminal peptides was visualized using the raincloud plot R tool (76).

For co-cultured MDA-MB-231/HMF cells, TMT labels (126, 127N, 127C, 128N; TMT 10-plex kit 90110 from Thermo Scientific) dissolved in DMSO were added in a 1:5 (total protein/ TMT label) mass ratio to one of the four samples (60 µg of total protein per condition) for 60 min. Labelling reactions were stopped with 5% hydroxylamine (Sigma) for 30 min, and the four samples were mixed and precipitated with cold methanol/acetone (8:1) (v/v). After two washes with cold methanol, the pellet was resuspended in 100mM HEPES at pH 8 at a final protein concentration of 2 mg/ml and digested with trypsin (trypsin/total protein (1:100); Trypsin V511A, Promega) overnight. N-terminal peptide enrichment was performed on the digested sample by removing the internal tryptic peptides with a 1:5 mass excess of dialyzed HPG-ALD polymer, desalted with a C18 spin column (Thermo Fisher Scientific). The eluate fraction was freeze-dried, resuspended in 0.1% FA and analysed by LC-MS/MS on a Q-Exactive HF mass spectrometer, as described above for ATOMS experiments except that the SwissProt 2019-12 Homo sapiens database release was used and that iTRAQ 8-plex was replaced by TMT 10-plex in the list of variable modifications. The ratios without pepstatin A/with pepstatin A were calculated for the two time points (0 min and 60 min) and ratios at 60 min were normalized to the ratios

at 0 min. Only peptides with N-terminal TMT labelling and ratios showing at least a two-fold change are indicated in Table 1.

Study approval

For TMA, TNBC samples were provided by the biological resource centre (Biobank number BB-0033-00059) after approval by the Montpellier Cancer Institute Institutional Review Board, following the Ethics and Legal national French regulations for patient information and consent. For TNBC cytosols, patient samples were processed according to the French Public Health Code (law n°2004-800, articles L. 1243-4 and R. 1243-61). The biological resources centre has been authorized (authorization number: AC-2008-700; Val d'Aurelle, ICM, Montpellier) to deliver human samples for scientific research. All patients were informed before surgery that their surgical specimens might be used for research purposes. The study approval for PDXs was previously published (40).

Construction of tissue microarrays

Tumor tissue blocks with enough material at gross inspection were selected from the Biological Resource Centre. After haematoxylin-eosin-safranin (HES) staining, the presence of tumor tissue in sections was evaluated by a pathologist. Two representative tumor areas, to be used for the construction of the TMAs, were identified on each slide. A manual arraying instrument (Manual Tissue Arrayer 1, Beecher Instruments, Sun Prairie, WI, USA) was used to extract two malignant cores (1 mm in diameter) from the two selected areas. When possible, normal breast epithelium was also sampled as internal control. After arraying completion, 4 µm sections were cut from the TMA blocks. One section was stained with HES and the others were used for IHC.

TMA immunohistochemistry

For SPARC and cath-D immunostaining, serial tumor sections from a TNBC TMA were incubated with 0.2 µg/ml anti-human SPARC mouse monoclonal antibody (clone AON-5031) for 30 min or with 0.4 µg/ml anti-human cath-D mouse monoclonal antibody (clone C-5) for 20 min after heat-induced antigen retrieval with the PTLink pre-treatment (Dako) and the High pH Buffer (Dako) and endogenous

peroxidase quenching with Flex Peroxidase Block (Dako). After two rinses in EnVision™ Flex Wash buffer (Dako), sections were incubated with a HRP-labelled polymer coupled to a secondary anti-mouse antibody (Flex® system, Dako) for 20 min, followed by incubation with 3,3'-diaminobenzidine as chromogen. Sections were counterstained with Flex Hematoxylin (Dako) and mounted after dehydration. Sections were analysed independently by two experienced pathologists, both blinded to the tumor characteristics and patient outcomes at the time of scoring. SPARC signal was scored as low (<50%), or high (>50%), and cath-D signal was scored as absent, low, medium (<50%), high, or very high (>50%) in cancer and stromal cells.

Fluorescence microscopy

Paraffin-embedded PDX1995 tissue sections were deparaffined, rehydrated, rinsed, and saturated in PBS with 5% FCS at 4°C overnight. Sections were co-incubated with 1.2 µg/ml anti-SPARC rabbit polyclonal antibody (Proteintech) and 0.4 µg/ml anti-cath-D mouse monoclonal antibody (clone C-5) followed by co-incubation with AlexaFluor 488-conjugated anti-rabbit IgG (1/400) and a Cy3-conjugated anti-mouse IgG (1/500). Nuclei were stained with 0.5 µg/ml Hoechst 33342. Sections were then imaged with a 63X Plan-Apochromat objective on z stacks with a Zeiss Axio Imager light microscope equipped with Apotome to eliminate out-of-focus fluorescence. For co-staining of SPARC/cath-D, series of three optical sections (0.25 µm thick) were collected and projected onto a single plane.

siRNA transfection

The siRNA duplex (21 nucleotides) against human cath-D siRNA (ID 4180) was purchased from Ambion (Austin, TX), and the firefly luciferase (Luc) siRNA (target sequence AACGUACGCGGAAUACUUCGA) was synthesized by MWG Biotech S.A (77). MDA-MB-231 cells in 6-well plates were transiently transfected with 4 µg human cath-D or Luc siRNA using Lipofectamine 2000 (Invitrogen). At 48h post-transfection, 200 000 siRNA-transfected MDA-MB-231 cells were plated with 100 000 HMFs in T25 cell culture flasks for co-culture experiments.

RT-qPCR

For gene expression analysis, fresh tumor tissues were homogenized in an Ultra-Turrax. RNA was isolated using the RNeasy Mini Kit (Qiagen, Hilden, Germany) and 1 µg of total RNA was reverse transcribed using the iScript™ cDNA Synthesis Kit (Bio-Rad, Feldkirchen, Germany). Real-time PCR was performed using Platinum SYBR Green qPCR Super Mix-UDG (Life Technologies, Darmstadt, Germany) on a CFX96 real-time PCR machine (Bio-Rad) with the following primers: *SPARC* forward: 5'-GCTGTGTTGGAAACGGAGTTG-3'; *SPARC* reverse: 5'-CTTGCCATGTGGGTTCTGACT-3'; *ACTB* (β-actin) forward: 5'-ACCCAGGCATTGCTGACAGG-3', *ACTB* reverse: 5'-GGACAGTGAGGCCAGGATGG-3'. *SPARC* expression data were normalized to *ACTB* expression.

Expression and purification of recombinant proteins

The cDNA encoding human SPARC (303 amino acids according to the GenBank reference NP_003109) and its truncated fragments were PCR-amplified using the pcDNA3.1-SPARC plasmid as template (78), cloned into pGEM®-T Easy Vector (Promega), and then into the pSec-Tag2/hygroA vector (Thermo Fisher Scientific) by *Not* I digestion. Orientation and sequence were verified (Supplementary Table S1). Human embryonic kidney 293 (HEK-293T) cells were stably transfected with the vectors using Lipofectamine 2000 (Invitrogen) according to the manufacturer's instructions, and were selected with 400 µg/ml hygromycin B Gold™ (Invivogen). The recombinant His-tagged proteins were purified from cell lysates on a nickel-chelating column (Ni-nitrilotriacetic acid agarose; His-select high flow nickel affinity gel; Sigma-Aldrich), as described previously (52). The isolated recombinant proteins were analysed by western blotting using anti-mouse Myc (clone 9B11) and anti-SPARC (clone AON-5031) antibodies and quantified using the Image J densitometric software (National Institutes of Health). To immunodeplete purified SPARC or its fragments, protein supernatants were incubated with an anti-Myc antibody (clone 9B11) overnight and protein G-Sepharose at 4°C for 4h, and supernatants were analysed by immunoblotting to validate SPARC depletion. SPARC-immunodepleted supernatants were used as internal controls in the biological assays.

Cell adhesion, migration, endothelial transmigration and invasion assays

Adhesion of MDA-MB-231 cells was assessed as described (52). Briefly, 96-well plates were coated with fibronectin (10 µg/ml; sc-29011; Santa Cruz Biotechnology) at 4°C overnight, and saturated with 1% BSA in PBS. MDA-MB-231 cells were detached with HyQTase (HyClone), washed in DMEM without FCS, and 1.5 10^5 cells were pre-incubated or not with SPARC or its cleaved fragments at room temperature for 10 min. Cells (5 10^4 cells) were plated and left in serum-free medium at 37°C for 30 min. Non-adherent cells were removed by floatation on a dense Percoll solution containing 3.33% NaCl (1.10 g/l), and adherent cells were fixed (10% [vol/vol] glutaraldehyde) using the buoyancy method (79). Cells were stained with 0.1% crystal violet, and absorbance was measured at 570 nm. For migration assays, 8-µm pore Transwell inserts in 24-well plates (polyvinyl pyrrolidone-free polycarbonate filter) (Corning Inc., Corning, NY, USA) were coated with 10 µg/ml fibronectin (500 ng) at 4°C for 24h. For invasion assays, 8-µm pore Transwell inserts were coated with Matrigel (100 µg, Corning). MDA-MB-231 cells (2 10^5 cells) were pre-incubated or not with SPARC or its cleaved fragments at room temperature for 10 min, and then plated (5 10^4 cells/well) in FCS-free DMEM on the coated insert in the upper chamber. For transmigration assay, 10^5 HUVECs were plated in the upper chamber of a gelatine-coated Transwell insert and grown in complete endothelial medium to confluence, as previously described (23). The endothelial monolayer was then incubated with human TNFα (10 ng/ml; PeproTech) for 16h. MDA-MB-231 cells (3 10^5 cells), pre-incubated or not with SPARC or its cleaved fragments at room temperature for 10 min, were then plated (10^5 cells/well) in FCS-free DMEM on top of the endothelial monolayer. In these different assays, DMEM supplemented with 10% FCS was used as chemoattractant in the bottom chamber. After 16h, non-migrating/non-invading/non-transmigrating cells on the apical side of each insert were scraped off with a cotton swab, and migration, invasion and transmigration were analysed with two methods: (1) migrating/invading/transmigrating cells were fixed in methanol, stained with 0.1% crystal violet for 30 min, rinsed in water, and imaged with an optical microscopy. Two images of the pre-set field per insert were captured (x100); (2) migrating/invading/transmigrating cells were incubated with 3-(4,5-dimethylthiazol-2-yl)-2,5-

diphenyltetrazolium bromide (MTT; 5 mg/ml, 1/10 volume; Sigma-Aldrich) added to the culture medium at 37°C for 4h. Then, the culture medium/MTT solution was removed and centrifuged at 10 000 rpm for 5 min. After centrifugation, cell pellets were suspended in DMSO. Concomitantly, 300 µl of DMSO was added to each well and thoroughly mixed for 5 min. The optical density values of stained cells (cell pellet and corresponding well) were measured using a microplate reader at 570 nm.

AUTHOR CONTRIBUTIONS

LBA, AM, DD, FD, CO, PR, TR, CM, ELC designed the experiments and prepared the manuscript. LBA, AM, TD, DD, FD, CD, FB, JSF, PFH, PR, TR, ELC performed the experiments. LBA, AM, DD, FD, JSF, SDM, PFH, CO, STD, WJ, SG, PR, TR, CM, ELC provided material and analysed data. LBA, AM, TC, TR, CM, ELC analysed data and proof-read and finalized the manuscript.

ACKNOWLEDGMENTS

This work was supported by a public grant overseen by the French National Research Agency (ANR) as part of the "Investissements d'Avenir" program (reference: LabEx MabImprove ANR-10-LABX-53-01), SIRIC Montpellier Cancer Grant INCa_Inserm_DGOS_12553, University of Montpellier, the associations 'Ligue Régionale du Gard', 'Ligue Régionale de l'Herault', 'Ligue Régionale de la Charente Maritime, and 'Association pour la Recherche sur le Cancer' (ARC). The work of TR was supported by the German Research Foundation (DFG) SFB 850 project B7, RE 1584/6-2, and GRK 2606. We thank Susanne Dollwet-Mack and Lisa Heß (Institute of Molecular Medicine and Cell Research, Freiburg, Germany) for helpful discussions and support. The authors acknowledge Biological Resources Centre from Montpellier Cancer Institute (ICM Biobank n° BB 0033 00059).

REFERENCES

1. Bianchini G, Balko JM, Mayer IA, Sanders ME, Gianni L. Triple-negative breast cancer: challenges and opportunities of a heterogeneous disease. Nature reviews Clinical oncology 2016;13(11):674-90.

2. Ferrandina G, Scambia G, Bardelli F, Benedetti Panici P, Mancuso S, Messori A. Relationship between cathepsin-D content and disease-free survival in node-negative breast cancer patients: a meta-analysis. Br J Cancer 1997;76(5):661-6.

3. Foekens JA, Look MP, Bolt-de Vries J, Meijer-van Gelder ME, van Putten WL, Klijn JG. Cathepsin-D in primary breast cancer: prognostic evaluation involving 2810 patients. Br J Cancer 1999;79(2):300-7.

4. Kang J, Yu Y, Jeong S, Lee H, Heo HJ, Park JJ, et al. Prognostic role of high cathepsin D expression in breast cancer: a systematic review and meta-analysis. Ther Adv Med Oncol 2020;12:1758835920927838.

5. Huang L, Liu Z, Chen S, Liu Y, Shao Z. A prognostic model for triple-negative breast cancer patients based on node status, cathepsin-D and Ki-67 index. PloS one 2013;8(12):e83081.

6. Mansouri H, Alcaraz LB, Mollevi C, Mallavialle A, Jacot W, Boissiere-Michot F, et al. Co-Expression of Androgen Receptor and Cathepsin D Defines a Triple-Negative Breast Cancer Subgroup with Poorer Overall Survival. Cancers (Basel) 2020;12(5).

7. Vignon F, Capony F, Chambon M, Freiss G, Garcia M, Rochefort H. Autocrine growth stimulation of the MCF 7 breast cancer cells by the estrogen-regulated 52 K protein. Endocrinology 1986;118(4):1537-45.

8. Hasilik A, von Figura K, Conzelmann E, Nehrkorn H, Sandhoff K. Lysosomal enzyme precursors in human fibroblasts. Activation of cathepsin D precursor in vitro and activity of beta-hexosaminidase A precursor towards ganglioside GM2. Eur J Biochem 1982;125(2):317-21.

9. Berchem G, Glondu M, Gleizes M, Brouillet JP, Vignon F, Garcia M, et al. Cathepsin-D affects multiple tumor progression steps in vivo: proliferation, angiogenesis and apoptosis. Oncogene 2002;21(38):5951-5.

10. Glondu M, Coopman P, Laurent-Matha V, Garcia M, Rochefort H, Liaudet-Coopman E. A mutated cathepsin-D devoid of its catalytic activity stimulates the growth of cancer cells. Oncogene 2001;20(47):6920-9.

11. Glondu M, Liaudet-Coopman E, Derocq D, Platet N, Rochefort H, Garcia M. Down-regulation of cathepsin-D expression by antisense gene transfer inhibits tumor growth and experimental lung metastasis of human breast cancer cells. Oncogene 2002;21(33):5127-34.

12. Ketterer S, Mitschke J, Ketscher A, Schlimpert M, Reichardt W, Baeuerle N, et al. Cathepsin D deficiency in mammary epithelium transiently stalls breast cancer by interference with mTORC1 signaling. Nature communications 2020;11(1):5133.

13. Beaujouin M, Prebois C, Derocq D, Laurent-Matha V, Masson O, Pattingre S, et al. Pro-cathepsin D interacts with the extracellular domain of the beta chain of LRP1 and promotes LRP1-dependent fibroblast outgrowth. Journal of cell science 2010;123(Pt 19):3336-46.

14. Laurent-Matha V, Maruani-Herrmann S, Prebois C, Beaujouin M, Glondu M, Noel A, et al. Catalytically inactive human cathepsin D triggers fibroblast invasive growth. J Cell Biol 2005;168(3):489-99.

15. Hu L, Roth JM, Brooks P, Luty J, Karpatkin S. Thrombin up-regulates cathepsin D which enhances angiogenesis, growth, and metastasis. Cancer Res 2008;68(12):4666-73.

16. Ashraf Y, Mansouri H, Laurent-Matha V, Alcaraz LB, Roger P, Guiu S, et al. Immunotherapy of triple-negative breast cancer with cathepsin D-targeting antibodies. J Immunother Cancer 2019;7(1):29.

17. Kleifeld O, Doucet A, Prudova A, Auf dem Keller U, Gioia M, Kizhakkedathu JN, et al. Identifying and quantifying proteolytic events and the natural N terminome by terminal amine isotopic labeling of substrates. Nat Protoc 2011;6(10):1578-611.

18. Laurent-Matha V, Huesgen PF, Masson O, Derocq D, Prebois C, Gary-Bobo M, et al. Proteolysis of cystatin C by cathepsin D in the breast cancer microenvironment. FASEB journal : official publication of the Federation of American Societies for Experimental Biology 2012.

19. Sage EH, Bornstein P. Extracellular proteins that modulate cell-matrix interactions. SPARC, tenascin, and thrombospondin. The Journal of biological chemistry 1991;266(23):14831-4.

20. Lane TF, Sage EH. The biology of SPARC, a protein that modulates cell-matrix interactions. FASEB journal : official publication of the Federation of American Societies for Experimental Biology 1994;8(2):163-73.

21. Brekken RA, Sage EH. SPARC, a matricellular protein: at the crossroads of cell-matrix. Matrix Biol 2000;19(7):569-80.

22. Murphy-Ullrich JE, Sage EH. Revisiting the matricellular concept. Matrix Biol 2014;37:1-14.

23. Tichet M, Prod'Homme V, Fenouille N, Ambrosetti D, Mallavialle A, Cerezo M, et al. Tumor-derived SPARC drives vascular permeability and extravasation through endothelial VCAM1 signalling to promote metastasis. Nature communications 2015;6:6993.

24. Hsiao YH, Lien HC, Hwa HL, Kuo WH, Chang KJ, Hsieh FJ. SPARC (osteonectin) in breast tumors of different histologic types and its role in the outcome of invasive ductal carcinoma. Breast J 2010;16(3):305-8.

25. Barth PJ, Moll R, Ramaswamy A. Stromal remodeling and SPARC (secreted protein acid rich in cysteine) expression in invasive ductal carcinomas of the breast. Virchows Archiv : an international journal of pathology 2005;446(5):532-6.

26. Podhajcer OL, Benedetti LG, Girotti MR, Prada F, Salvatierra E, Llera AS. The role of the matricellular protein SPARC in the dynamic interaction between the tumor and the host. Cancer metastasis reviews 2008;27(4):691-705.

27. Nagaraju GP, Dontula R, El-Rayes BF, Lakka SS. Molecular mechanisms underlying the divergent roles of SPARC in human carcinogenesis. Carcinogenesis 2014;35(5):967-73.

28. Briggs J, Chamboredon S, Castellazzi M, Kerry JA, Bos TJ. Transcriptional upregulation of SPARC, in response to c-Jun overexpression, contributes to increased motility and invasion of MCF7 breast cancer cells. Oncogene 2002;21(46):7077-91.

29. Watkins G, Douglas-Jones A, Bryce R, Mansel RE, Jiang WG. Increased levels of SPARC (osteonectin) in human breast cancer tissues and its association with clinical outcomes. Prostaglandins Leukot Essent Fatty Acids 2005;72(4):267-72.

30. Sangaletti S, Tripodo C, Santangelo A, Castioni N, Portararo P, Gulino A, et al. Mesenchymal Transition of High-Grade Breast Carcinomas Depends on Extracellular Matrix Control of Myeloid Suppressor Cell Activity. Cell Rep 2016;17(1):233-48.

31. Zhu A, Yuan P, Du F, Hong R, Ding X, Shi X, et al. SPARC overexpression in primary tumors correlates with disease recurrence and overall survival in patients with triple negative breast cancer. Oncotarget 2016;7(47):76628-34.

32. Guttlein LN, Benedetti LG, Fresno C, Spallanzani RG, Mansilla SF, Rotondaro C, et al. Predictive Outcomes for HER2-enriched Cancer Using Growth and Metastasis Signatures Driven By SPARC. Mol Cancer Res 2017;15(3):304-16.

33. McQuerry JA, Jenkins DF, Yost SE, Zhang Y, Schmolze D, Johnson WE, et al. Pathway activity profiling of growth factor receptor network and stemness pathways differentiates metaplastic breast cancer histological subtypes. BMC cancer 2019;19(1):881.

34. Dhanesuan N, Sharp JA, Blick T, Price JT, Thompson EW. Doxycycline-inducible expression of SPARC/Osteonectin/BM40 in MDA-MB-231 human breast cancer cells results in growth inhibition. Breast cancer research and treatment 2002;75(1):73-85.

35. Ma J, Gao S, Xie X, Sun E, Zhang M, Zhou Q, et al. SPARC inhibits breast cancer bone metastasis and may be a clinical therapeutic target. Oncol Lett 2017;14(5):5876-82.

36. Koblinski JE, Kaplan-Singer BR, VanOsdol SJ, Wu M, Engbring JA, Wang S, et al. Endogenous osteonectin/SPARC/BM-40 expression inhibits MDA-MB-231 breast cancer cell metastasis. Cancer Res 2005;65(16):7370-7.

37. Clark CJ, Sage EH. A prototypic matricellular protein in the tumor microenvironment--where there's SPARC, there's fire. J Cell Biochem 2008;104(3):721-32.

38. Bradshaw AD, Sage EH. SPARC, a matricellular protein that functions in cellular differentiation and tissue response to injury. J Clin Invest 2001;107(9):1049-54.

39. Gyorffy B, Lanczky A, Eklund AC, Denkert C, Budczies J, Li Q, et al. An online survival analysis tool to rapidly assess the effect of 22,277 genes on breast cancer prognosis using microarray data of 1,809 patients. Breast cancer research and treatment 2010;123(3):725-31.

40. du Manoir S, Orsetti B, Bras-Goncalves R, Nguyen TT, Lasorsa L, Boissiere F, et al. Breast tumor PDXs are genetically plastic and correspond to a subset of aggressive cancers prone to relapse. Molecular oncology 2014;8(2):431-43.

41. Gilles C, Bassuk JA, Pulyaeva H, Sage EH, Foidart JM, Thompson EW. SPARC/osteonectin induces matrix metalloproteinase 2 activation in human breast cancer cell lines. Cancer Res 1998;58(23):5529-36.

42. Kleifeld O, Doucet A, auf dem Keller U, Prudova A, Schilling O, Kainthan RK, et al. Isotopic labeling of terminal amines in complex samples identifies protein N-termini and protease cleavage products. Nat Biotechnol 2010;28(3):281-8.

43. Griffiths JR, McIntyre DJ, Howe FA, Stubbs M. Why are cancers acidic? A carrier-mediated diffusion model for H+ transport in the interstitial fluid. Novartis Found Symp 2001;240:46-62; discussion 62-7, 152-3.

44. Ketscher A, Ketterer S, Dollwet-Mack S, Reif U, Reinheckel T. Neuroectoderm-specific deletion of cathepsin D in mice models human inherited neuronal ceroid lipofuscinosis type 10. Biochimie 2016;122:219-26.

45. Guy CT, Cardiff RD, Muller WJ. Induction of mammary tumors by expression of polyomavirus middle T oncogene: a transgenic mouse model for metastatic disease. Mol Cell Biol 1992;12(3):954-61.

46. Murphy-Ullrich JE, Lane TF, Pallero MA, Sage EH. SPARC mediates focal adhesion disassembly in endothelial cells through a follistatin-like region and the Ca(2+)-binding EF-hand. J Cell Biochem 1995;57(2):341-50.

47. Seux M, Peuget S, Montero MP, Siret C, Rigot V, Clerc P, et al. TP53INP1 decreases pancreatic cancer cell migration by regulating SPARC expression. Oncogene 2011;30(27):3049-61.

48. Tseng C, Kolonin MG. Proteolytic Isoforms of SPARC Induce Adipose Stromal Cell Mobilization in Obesity. Stem cells 2016;34(1):174-90.

49. Murphy-Ullrich JE. The de-adhesive activity of matricellular proteins: is intermediate cell adhesion an adaptive state? J Clin Invest 2001;107(7):785-90.

50. Palecek SP, Loftus JC, Ginsberg MH, Lauffenburger DA, Horwitz AF. Integrin-ligand binding properties govern cell migration speed through cell-substratum adhesiveness. Nature 1997;385(6616):537-40.

51. Lethias C, Elefteriou F, Parsiegla G, Exposito JY, Garrone R. Identification and characterization of a conformational heparin-binding site involving two fibronectin type III modules of bovine tenascin-X. The Journal of biological chemistry 2001;276(19):16432-8.

52. Alcaraz LB, Exposito JY, Chuvin N, Pommier RM, Cluzel C, Martel S, et al. Tenascin-X promotes epithelial-to-mesenchymal transition by activating latent TGF-beta. J Cell Biol 2014;205(3):409-28.

53. Sage H, Vernon RB, Funk SE, Everitt EA, Angello J. SPARC, a secreted protein associated with cellular proliferation, inhibits cell spreading in vitro and exhibits Ca+2-dependent binding to the extracellular matrix. J Cell Biol 1989;109(1):341-56.

54. Eswaran J, Cyanam D, Mudvari P, Reddy SD, Pakala SB, Nair SS, et al. Transcriptomic landscape of breast cancers through mRNA sequencing. Scientific reports 2012;2:264.

55. Dunn BM, Hung S. The two sides of enzyme-substrate specificity: lessons from the aspartic proteinases. Biochimica et biophysica acta 2000;1477(1-2):231-40.

56. Lane TF, Iruela-Arispe ML, Johnson RS, Sage EH. SPARC is a source of copper-binding peptides that stimulate angiogenesis. J Cell Biol 1994;125(4):929-43.

57. Sasaki T, Gohring W, Mann K, Maurer P, Hohenester E, Knauper V, et al. Limited cleavage of extracellular matrix protein BM-40 by matrix metalloproteinases increases its affinity for collagens. The Journal of biological chemistry 1997;272(14):9237-43.

58. Sage EH, Reed M, Funk SE, Truong T, Steadele M, Puolakkainen P, et al. Cleavage of the matricellular protein SPARC by matrix metalloproteinase 3 produces polypeptides that influence angiogenesis. The Journal of biological chemistry 2003;278(39):37849-57.

59. Kehlet SN, Manon-Jensen T, Sun S, Brix S, Leeming DJ, Karsdal MA, et al. A fragment of SPARC reflecting increased collagen affinity shows pathological relevance in lung cancer - implications of a new collagen chaperone function of SPARC. Cancer biology & therapy 2018;19(10):904-12.

60. Podgorski I, Linebaugh BE, Koblinski JE, Rudy DL, Herroon MK, Olive MB, et al. Bone marrow-derived cathepsin K cleaves SPARC in bone metastasis. The American journal of pathology 2009;175(3):1255-69.

61. Edwards NJ, Oberti M, Thangudu RR, Cai S, McGarvey PB, Jacob S, et al. The CPTAC Data Portal: A Resource for Cancer Proteomics Research. J Proteome Res 2015;14(6):2707-13.

62. Campo McKnight DA, Sosnoski DM, Koblinski JE, Gay CV. Roles of osteonectin in the migration of breast cancer cells into bone. J Cell Biochem 2006;97(2):288-302.

63. Hohenester E, Maurer P, Hohenadl C, Timpl R, Jansonius JN, Engel J. Structure of a novel extracellular Ca(2+)-binding module in BM-40. Nature structural biology 1996;3(1):67-73.

64. Dejeans N, Pluquet O, Lhomond S, Grise F, Bouchecareilh M, Juin A, et al. Autocrine control of glioma cells adhesion and migration through IRE1alpha-mediated cleavage of SPARC mRNA. Journal of cell science 2012;125(Pt 18):4278-87.

65. Busch E, Hohenester E, Timpl R, Paulsson M, Maurer P. Calcium affinity, cooperativity, and domain interactions of extracellular EF-hands present in BM-40. The Journal of biological chemistry 2000;275(33):25508-15.

66. Lane TF, Sage EH. Functional mapping of SPARC: peptides from two distinct Ca+(+)-binding sites modulate cell shape. J Cell Biol 1990;111(6 Pt 2):3065-76.

67. Yost JC, Sage EH. Specific interaction of SPARC with endothelial cells is mediated through a carboxyl-terminal sequence containing a calcium-binding EF hand. The Journal of biological chemistry 1993;268(34):25790-6.

68. Kelly KA, Allport JR, Yu AM, Sinh S, Sage EH, Gerszten RE, et al. SPARC is a VCAM-1 counter-ligand that mediates leukocyte transmigration. J Leukoc Biol 2007;81(3):748-56.

69. Gerarduzzi C, Hartmann U, Leask A, Drobetsky E. The Matrix Revolution: Matricellular Proteins and Restructuring of the Cancer Microenvironment. Cancer Res 2020;80(13):2705-17.

70. Sevenich L, Werner F, Gajda M, Schurigt U, Sieber C, Muller S, et al. Transgenic expression of human cathepsin B promotes progression and metastasis of polyoma-middle-T-induced breast cancer in mice. Oncogene 2011;30(1):54-64.

71. Saadoun H, Lamy PJ, Thezenas S, Pouderoux S, Bibeau F, Montels F, et al. Prognostic impact of the inclusion of uPA/PAI-1 tumor levels in the current adjuvant treatment decision-making for early breast cancer. Future oncology 2014;10(2):195-209.

72. Delolme F, Anastasi C, Alcaraz LB, Mendoza V, Vadon-Le Goff S, Talantikite M, et al. Proteolytic control of TGF-beta co-receptor activity by BMP-1/tolloid-like proteases revealed by quantitative iTRAQ proteomics. Cell Mol Life Sci 2015;72(5):1009-27.

73. Heumuller SE, Talantikite M, Napoli M, Armengaud J, Morgelin M, Hartmann U, et al. C-terminal proteolysis of the collagen VI alpha3 chain by BMP-1 and proprotein convertase(s) releases endotrophin in fragments of different sizes. The Journal of biological chemistry 2019;294(37):13769-80.

74. Craig R, Beavis RC. TANDEM: matching proteins with tandem mass spectra. Bioinformatics 2004;20(9):1466-7.

75. auf dem Keller U, Prudova A, Gioia M, Butler GS, Overall CM. A statistics-based platform for quantitative N-terminome analysis and identification of protease cleavage products. Mol Cell Proteomics 2010;9(5):912-27.

76. Allen M, Poggiali D, Whitaker K, Marshall TR, Kievit RA. Raincloud plots: a multi-platform tool for robust data visualization. Wellcome Open Res 2019;4:63.

77. Bach AS, Derocq D, Laurent-Matha V, Montcourrier P, Sebti S, Orsetti B, et al. Nuclear cathepsin D enhances TRPS1 transcriptional repressor function to regulate cell cycle progression and transformation in human breast cancer cells. Oncotarget 2015;6(29):28084-103.

78. Fenouille N, Puissant A, Tichet M, Zimniak G, Abbe P, Mallavialle A, et al. SPARC functions as an anti-stress factor by inactivating p53 through Akt-mediated MDM2 phosphorylation to promote melanoma cell survival. Oncogene 2011;30(49):4887-900.

79. Goodwin AE, Pauli BU. A new adhesion assay using buoyancy to remove non-adherent cells. J Immunol Methods 1995;187(2):213-9.

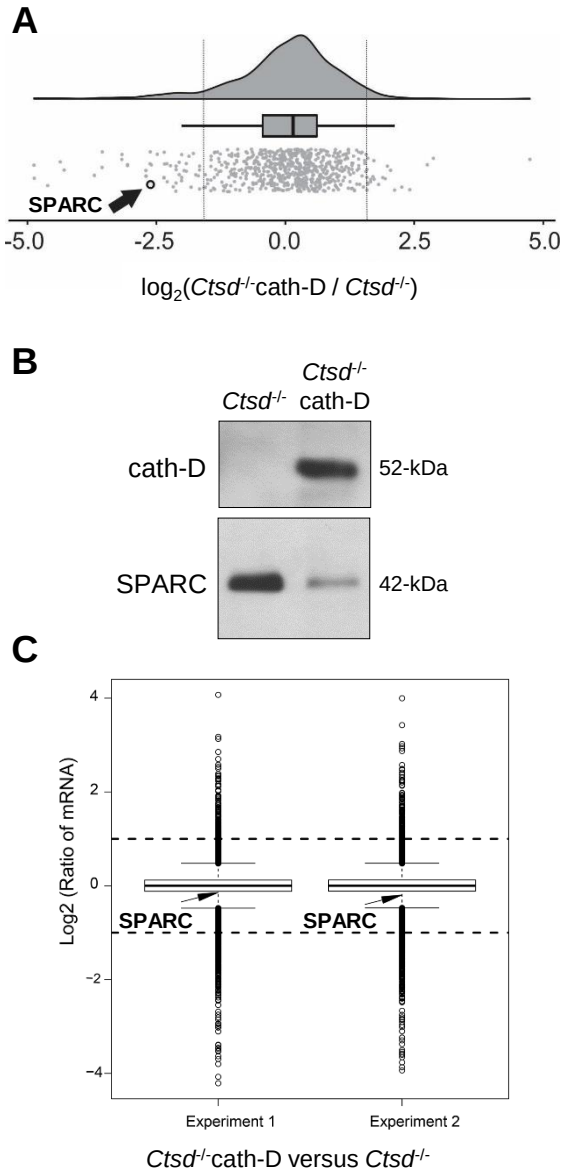

Fig. 1. SPARC analysis in *Ctsd*$^{-/-}$ MEFs transfected with human cath-D

(A) TAILS-based identification of protein N-termini affected by *Ctsd* deficiency. Comparison of the amounts of protein N termini in the secretomes of cath-D-deficient MEFs transfected with a plasmid encoding human cath-D (*Ctsd*$^{-/-}$cath-D) or empty vector (*Ctsd*$^{-/-}$). The distribution of 700 quantified N-terminal peptides was visualized as a raincloud plot that includes the distribution of individual N-terminal peptide ratios, a boxplot, and the probability distribution. Dashed lines indicate the 3-fold change in abundance (log2 <-1.58 or >1.58) chosen as cut-off for N-termini considered as severely affected by cath-D expression. The arrow indicates the SPARC peptide LDSELTEFPLR [156-166].

(B) Effect of *Ctsd* deficiency on SPARC protein level. Secretomes (30 µg) of *Ctsd*$^{-/-}$ and *Ctsd*$^{-/-}$cath-D MEFs were separated on 13.5% SDS-PAGE followed by immunoblotting with anti-cath-D (clone 49, #610801) and anti-SPARC (clone AON-5031) antibodies.

(C) Effect of *Ctsd* deficiency on *Sparc* mRNA level by transcriptomic analysis. The boxplots show the distribution of the expression values for all mRNAs (in log2 of ratio) in *Ctsd*$^{-/-}$cath-D and *Ctsd*$^{-/-}$ MEFs for two independent experiments. Arrows indicate *Sparc* expression values (0.91 and 0.87 on a linear scale, corresponding to -0.14 and -0.19 in the log2 scale). In these two experiments, *Sparc* mRNA showed a minimal deviation from the threshold (fold change of 2 or 1/2; i.e. log2(R)+1 or -1) commonly used to consider a gene as up- or down-regulated, and indicated by the dashed lines.

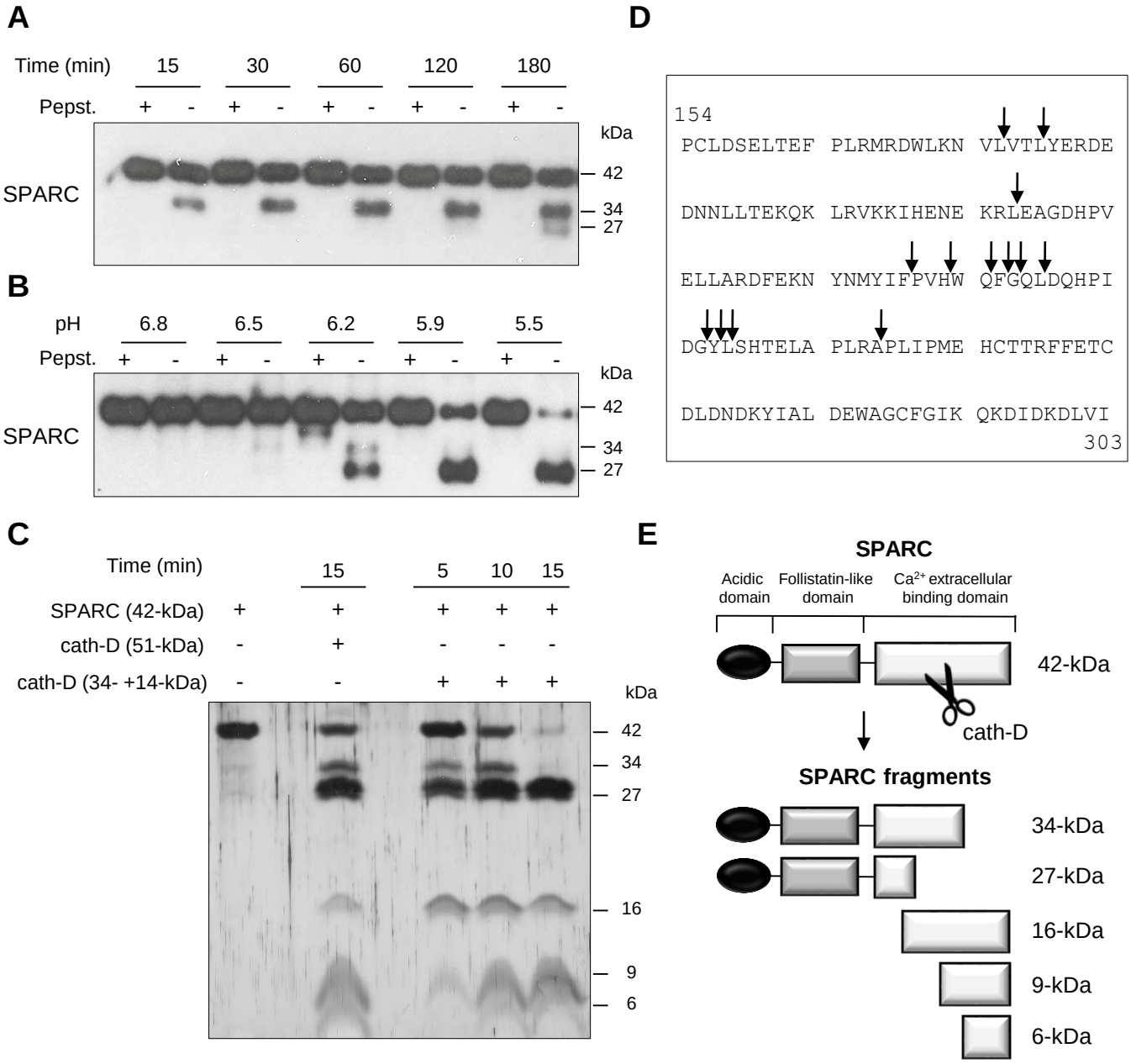

Fig. 2. Cleavage of human SPARC in its extracellular Ca^{2+} binding domain by human cath-D at acidic pH

(A) Time-course of cath-D-induced SPARC cleavage. Recombinant human FL SPARC was incubated with auto-activated cath-D in cleavage buffer at pH 5.9 with or without pepstatin A (Pepst.) at 37°C for the indicated times. SPARC cleavage was analysed by 13.5% SDS-PAGE and immunoblotting with an anti-SPARC monoclonal antibody (clone AON-5031).

(B) pH dependence of cath-D-induced SPARC cleavage. Recombinant human FL SPARC was incubated with auto-activated cath-D in cleavage buffer with or without pepstatin A (Pepst.) at the indicated pH at 37°C overnight. SPARC cleavage was analysed as in (A).

(C) Detection of the cath-D-induced SPARC fragments by silver staining. Recombinant SPARC was incubated with recombinant auto-activated pseudo-cath-D (51-kDa) or fully-mature cath-D (34+14-kDa) at pH 5.9 for the indicated times. SPARC cleavage was analysed by 17% SDS-PAGE and silver staining.

(D) Cleavage sites by cath-D in SPARC extracellular Ca^{2+} binding domain. The entire C-terminal extracellular Ca^{2+} binding domain of human SPARC (amino acids 154-303) is shown. SPARC cleaved peptides generated in the extracellular Ca^{2+} binding domain by auto-activated pseudo-cath-D (51-kDa) and fully-mature (34+14-kDa) cath-D at pH 5.9 were resolved by iTRAQ-ATOMS. Arrows, cleavage sites.

(E) Schematic representation of the SPARC fragments generated by cath-D according to (C) and (D).

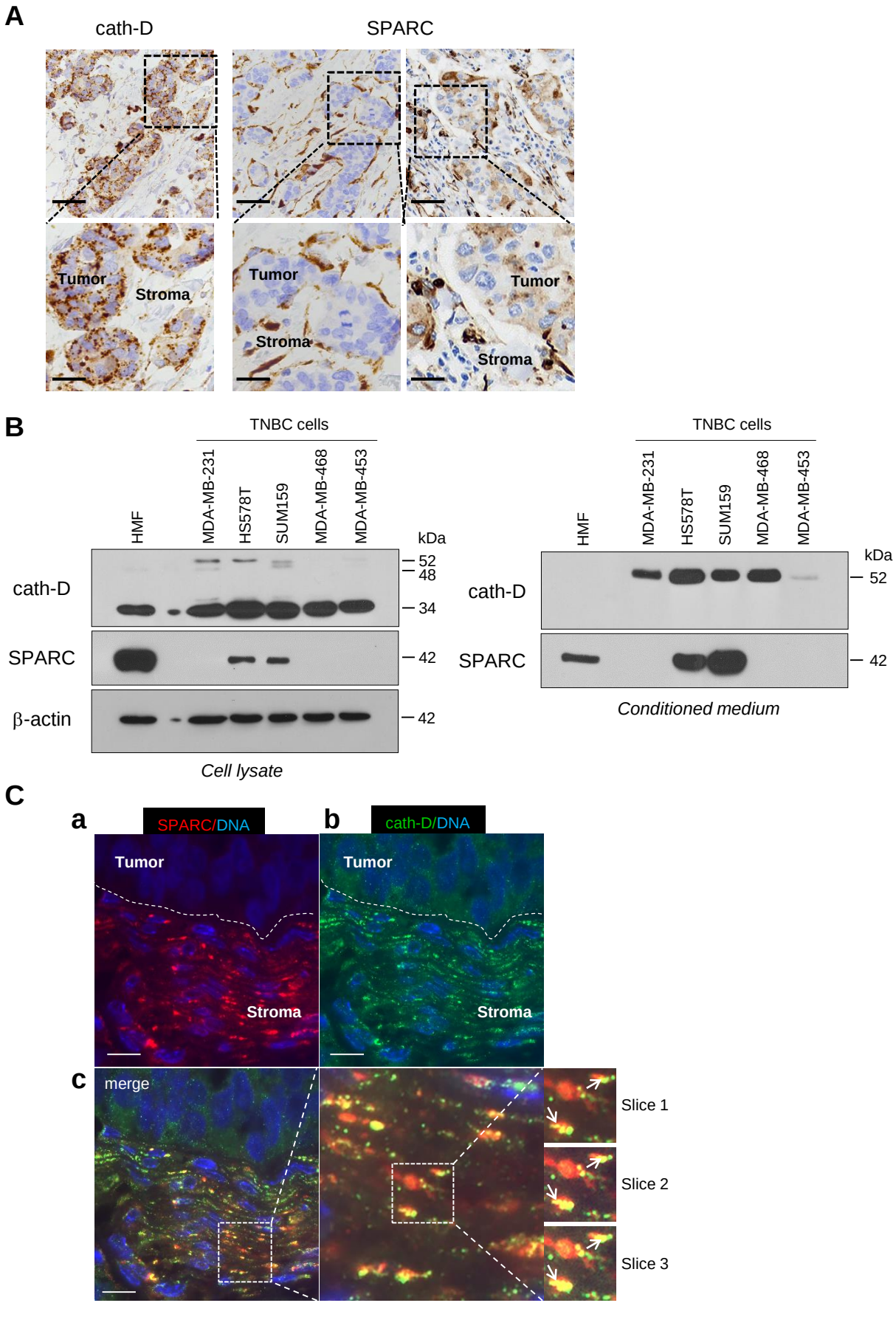

Fig. 3. Expression and co-localization of SPARC and cath-D in TNBC

Fig. 3. Expression and co-localization of SPARC and cath-D in TNBC

(A) SPARC and cath-D in a TNBC TMA. Representative images of SPARC and cath-D expression analysed in a TNBC TMA (n=147 samples) using anti–SPARC (clone AON-5031) and anti-cath-D (clone C-5) monoclonal antibodies. Scale bars, 50 µm (top panels) and 20 µm (bottom panels; higher magnifications of the boxed regions).

(B) SPARC and cath-D expression and secretion in TNBC cell lines and breast fibroblasts. Whole cell extracts (10 µg proteins) (left panel) and 24-hour conditioned media in the absence of FCS (40 µl) (right panel) were separated by 13.5% SDS-PAGE and analysed by immunoblotting with anti-cath-D antibodies for cellular (clone 49, #610801) and secreted cath-D (H-75), respectively, and anti-SPARC (clone AON-5031) antibodies. β-actin, loading control.

(C) Co-localization of SPARC and cath-D in TNBC PDX. PDX 1995 tumor sections were co-incubated with an anti-SPARC polyclonal antibody (Proteintech) (red; panel a) and an anti-cath-D monoclonal antibody (C-5) (green; panel b). Nuclei were stained with 0.5 µg/ml Hoechst 33342 (blue). Panel c (left): SPARC, cath-D and Hoechst 33342 merge. Panel c (middle): higher magnification of the box on the left. Panel c (right): higher magnifications (Z projections of 3 x 0.25 µm slices). Arrows indicate SPARC and cath-D co-localization. Scale bar, 10 µm.

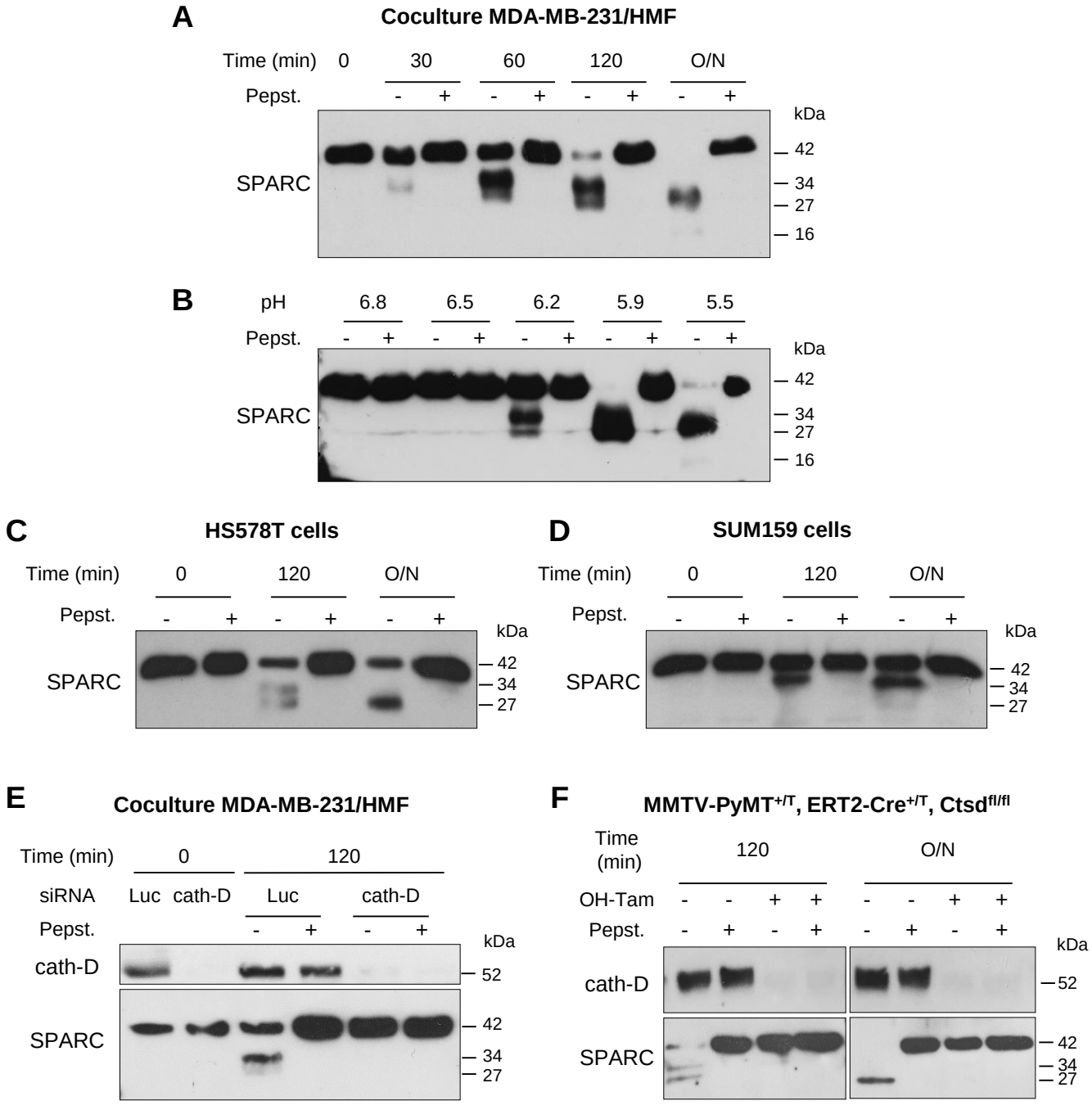

Fig. 4. Limited proteolysis of fibroblast- and cancer-derived SPARC by cath-D secreted by TNBC and mouse breast cancer cells at acidic pH

Fig. 4. Limited proteolysis of fibroblast- and cancer-derived SPARC by cath-D secreted by TNBC and mouse breast cancer cells at acidic pH

(A) Time-course of SPARC degradation in the MDA-MB-231/HMF co-culture MDA-MB-231 TNBC cells and HMFs were co-cultured in FCS-free DMEM without sodium bicarbonate and phenol red and buffered with 50 mM HEPES [pH 7] at 37°C for 24h. The 24h conditioned medium from co-cultured MDA-MB-231/HMFs was incubated at 37°C in cleavage buffer with or without pepstatin A (Pepst.) at pH 5.5 for the indicated times. SPARC cleavage in conditioned medium was analysed by 13.5% SDS-PAGE and immunoblotting with an anti-SPARC polyclonal antibody (Proteintech). O/N, overnight.

(B) Influence of the milieu acidity on SPARC degradation in the MDA-MB-231/HMF co-culture. MDA-MB-231 TNBC cells and HMFs were co-cultured as in (A). The 24-hour conditioned medium from co-cultured MDA-MB-231/HMFs was incubated at 37°C in cleavage buffer with or without pepstatin A at the indicated pH overnight. SPARC cleavage was analysed as described in (A).

(C and D) Time-course of SPARC cleavage in conditioned medium. HS578T TNBC cells (C) and SUM159 TNBC cells (D) were cultured in FCS-free DMEM without sodium bicarbonate and phenol red and buffered with 50 mM HEPES [pH 7] at 37°C for 24h.The 24h conditioned medium was incubated at 37°C in cleavage buffer with or without pepstatin A at pH 5.5 for the indicated times. SPARC cleavage was analysed as described in (A).

(E) SPARC cleavage by cath-D secreted by MDA-MB-231 cells. MDA-MB-231 cells were transfected with Luc or cath-D siRNAs. At 48h post-transfection, siRNA-transfected MDA-MB-231 cells were co-cultured with HMFs as described in (A). Then, the 24-hour conditioned media from co-cultured siRNA-transfected MDA-MB-231/HMFs were incubated at 37°C in cleavage buffer with or without pepstatin A at pH 5.5 for 120 min. Cath-D secretion by siRNA-transfected MDA-MB-231 cells was analysed with an anti-cath-D antibody (H-75). SPARC cleavage was analysed as described in (A).

(F) SPARC cleavage by cath-D secreted by inducible *Ctsd* knock-out MMTV-PyMT mammary tumor cells. Inducible *Ctsd* knock-out MMTV-PyMT breast cancer cells were incubated or not with 4-hydroxytamoxifen (OH-Tam; 3 μM) for 4 days to induce *Ctsd* knock-out. Then, cells were cultured in FCS-free DMEM without sodium bicarbonate and phenol red and buffered with 50 mM HEPES [pH 7] at 37°C for 24h. This 24h conditioned medium conditioned medium was incubated at 37°C in cleavage buffer with or without pepstatin A at pH 5.5 for 120 min or O/N. Cath-D secretion was analysed with an anti-cath-D antibody (AF1029). SPARC cleavage was analysed as described in (A).

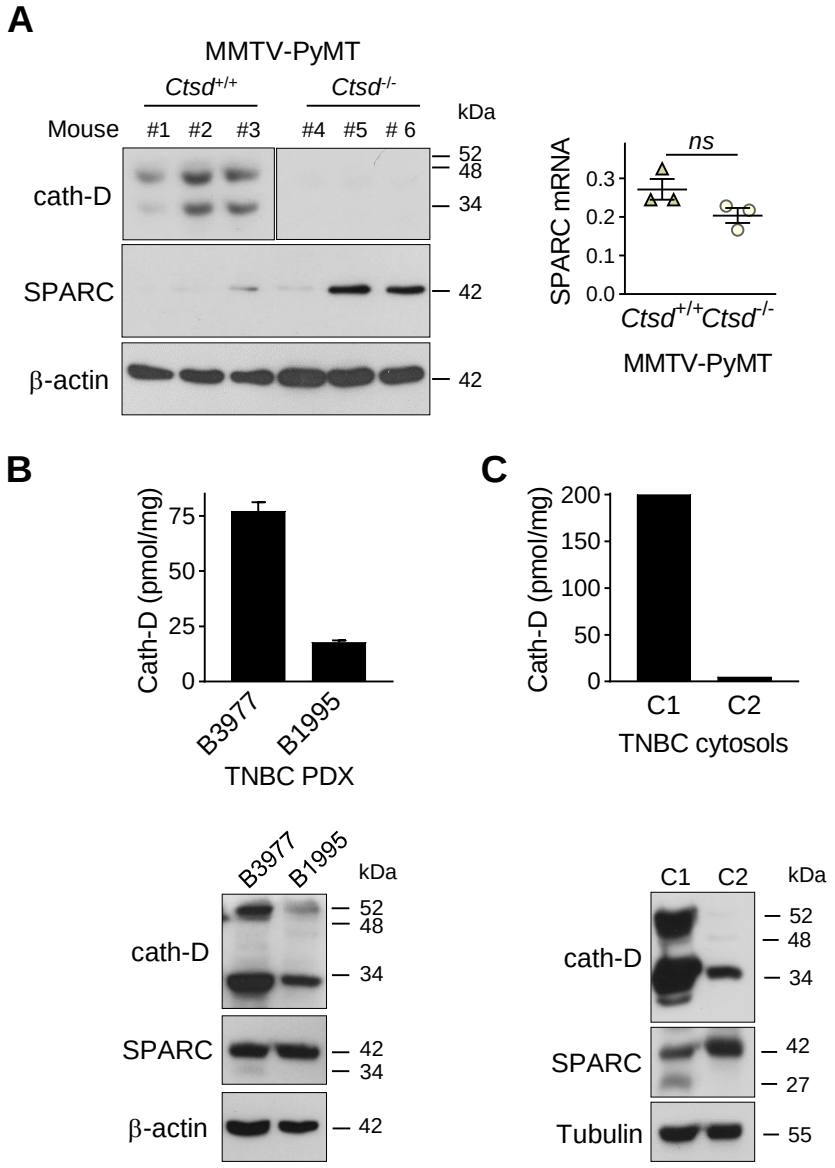

Fig. 5. Detection of FL SPARC and its cleaved fragments in mammary tumors

(A) SPARC expression in mammary tumors from MMTV-PyMT *Ctsd* knock-out mice. Left panel, whole cytosols (40 µg) of mammary tumors from MMTV-PyMT$^{Ctsd+/+}$ (N°1-3) and MMTV-PyMT$^{Ctsd-/-}$ (*Ctsd* knock-down in the mammary gland) (N°4-6) mice were analysed by 13.5% SDS-PAGE and immunoblotting with an anti-mouse cath-D monoclonal (clone 49, #610801) and anti-SPARC monoclonal antibody (AON-5031). β-actin, loading control. Right panel, total RNA was extracted from mammary tumors from MMTV-PyMT$^{Ctsd+/+}$ (N°1-3) and MMTV-PyMT$^{Ctsd-/-}$ (N°4-6) mice. *Sparc* expression was analysed by RT-qPCR. *P*=0.1 (Student's *t*-test).

(B and C) SPARC expression in TNBC PDXs and TNBC biopsies. Top panels, cath-D expression was determined in whole cytosols from two TNBC PDXs (B) and two TNBC biopsies (C) by sandwich ELISA with the immobilized anti-human cath-D D7E3 antibody and the anti-human cath-D M1G8 antibody coupled to HRP. Bottom panels, whole cytosols (40 µg) from these PDXs (B) and TNBC biopsies (C) were analysed by 13.5% SDS-PAGE and immunoblotting with anti-cath-D (H-75) and anti-SPARC (Proteintech) polyclonal antibodies. β-actin (B) and tubulin (C), loading controls.

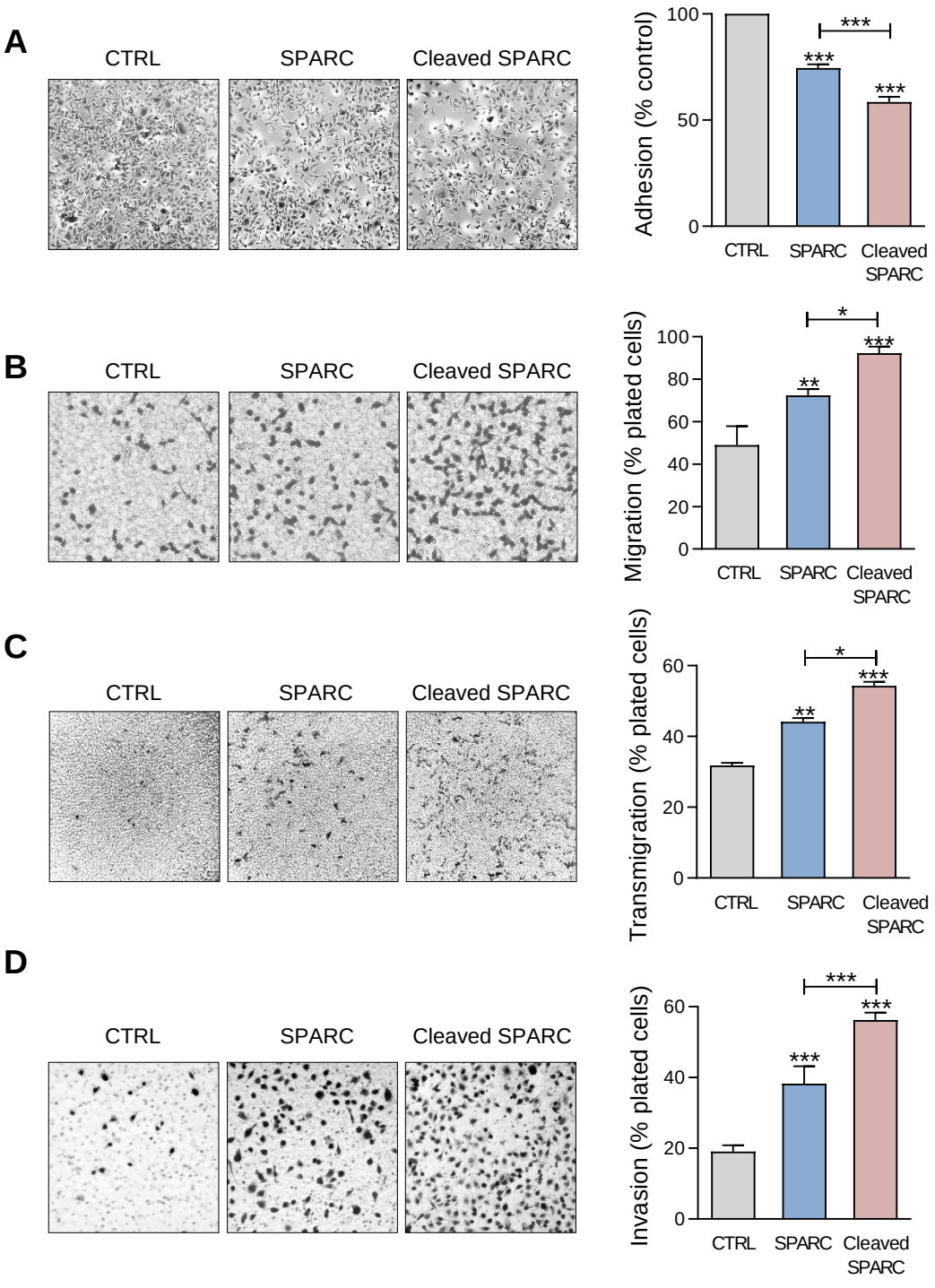

Fig. 6. Effects of FL SPARC and cath-D-induced cleaved SPARC fragments on adhesion, migration, transmigration and invasion of TNBC cells

Fig. 6. Effects of FL SPARC and cath-D-induced cleaved SPARC fragments on adhesion, migration, transmigration and invasion of TNBC cells

(A) Cell adhesion. MDA-MB-231 cells were let to adhere for 30 min on a fibronectin matrix in the absence or presence of recombinant FL SPARC (SPARC), or recombinant cath-D-induced cleaved SPARC fragments (cleaved SPARC) at the final concentration of 240 nM. Left panels, representative images of adherent cells. Right panel, adherent cells were stained with crystal violet, and adhesion was quantified at 570 nm. CTRL, PBS in cleavage buffer. Data are the mean ± SD (n=3); ***, $p<0.001$, ANOVA and Bonferroni's post hoc test. Similar results were obtained in four independent experiments.

(B) Cell migration. MDA-MB-231 cells were let to migrate for 16h on a fibronectin matrix in the absence or presence of recombinant FL SPARC, or cleaved SPARC at a final concentration of 240 nM. Left panels, representative images of migrating cells. Right panel, migrating cells were quantified by MTT staining and absorbance was read at 570 nm. CTRL, PBS in cleavage buffer. Data are the mean ± SD (n=3); *, $p<0.05$; **, $p<0.01$; ***, $p<0.001$, ANOVA and Bonferroni's post hoc test. Similar results were obtained in three **independent experiments.**

(C) Endothelial transmigration. MDA-MB-231 cells were let to transmigrate for 16h through a HUVEC monolayer in the absence or presence of recombinant FL SPARC, or cleaved SPARC at a final concentration of 240 nM. Left panels, representative images of transmigrating cells. Right panel, transmigrating cells were stained with MTT and quantified at 570 nm. CTRL, PBS in cleavage buffer. Data are the mean ± SD (n=3); *, $p<0.05$, **, $p<0.01$, ***, $p<0.001$, ANOVA and Bonferroni's post hoc test. Similar results were obtained in two independent experiments.

(D) Cell invasion. MDA-MB-231 cells were let to invade for 16h on a Matrigel matrix in the absence or presence of recombinant FL SPARC, or cleaved SPARC at a final concentration of 240 nM. Left panels, representative images of invading cells. Right panel, invading cells were stained with MTT and quantified at 570 nm. CTRL, PBS in cleavage buffer. Data are the mean ± SD (n=3); ***, $p<0.001$, ANOVA and Bonferroni's post hoc test. Similar results were obtained in three independent experiments.

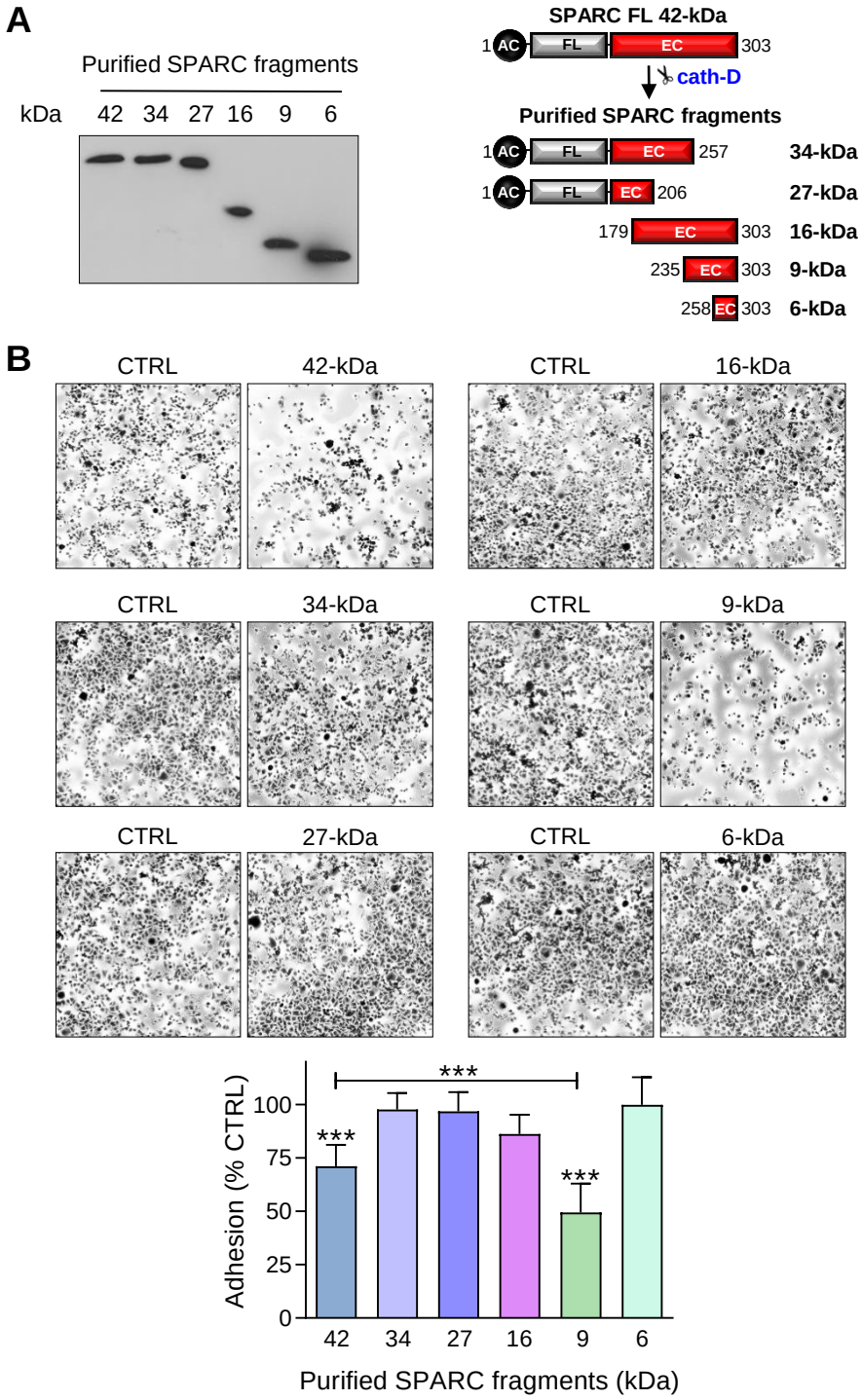

Fig. 7. Effect of FL SPARC and cath-D-induced cleaved SPARC fragments on TNBC cell adhesion

Fig. 7. Effect of FL SPARC and cath-D-induced cleaved SPARC fragments on TNBC cell adhesion
(A) Production of Myc/His tagged FL SPARC, and Myc/His tagged 34-, 27-, 16-, 9-, and 6-kDa SPARC fragments. Left panel, equimolar concentrations (240 nM each) of purified Myc/His tagged FL SPARC and SPARC fragments were analysed by SDS-PAGE (17%) and immunoblotting with an anti-Myc antibody (clone 9B11). Right panel, schematic representation of the purified Myc/His tagged SPARC fragments. AC, acidic domain; FL, follistatin-like domain; EC, Ca^{2+}-extracellular binding domain.
(B) Cell adhesion. MDA-MB-231 cells were let to adhere for 30 min on a fibronectin matrix in the presence of purified Myc/His tagged FL SPARC, or individual Myc/His tagged SPARC fragments (34-, 27-, 16-, 9-, and 6-kDa) at an equimolar final concentration (240 nM each). Upper panels, representative images of adherent cells stained with crystal violet after incubation with the indicated SPARC variants. Lower panel, cell adhesion was quantified as described in Fig. 6A and expressed as percentage relative to the value in control (SPARC-immunodepleted control for each SPARC fragment). Data are the mean ± SD of three independent experiments; ***, $p<0.001$, ANOVA and Bonferroni's post hoc test.

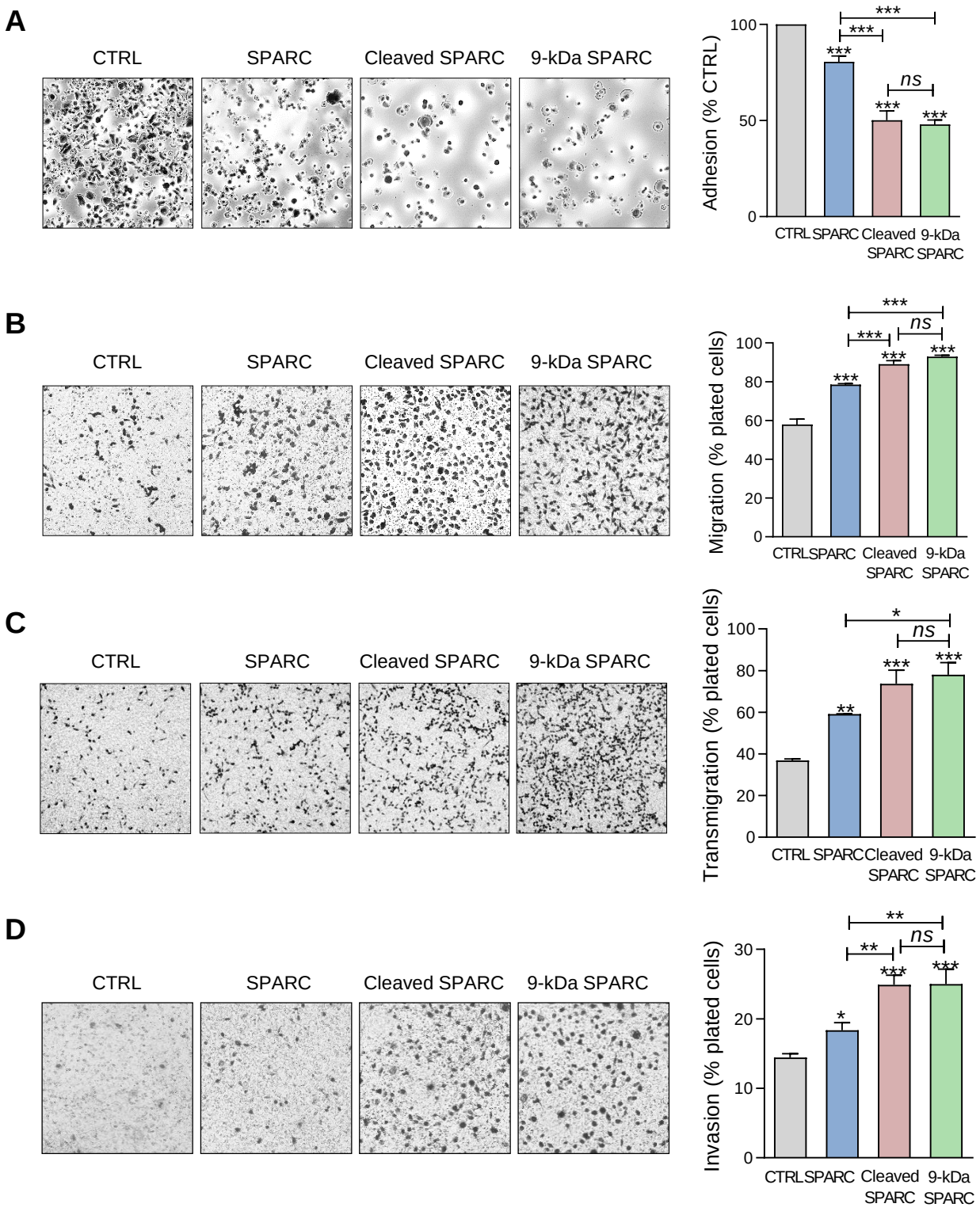

Fig. 8. Effects of the 9-kDa C-terminal SPARC fragment on TNBC cell adhesion, migration, transmigration and invasion

Fig. 8. Effects of the 9-kDa C-terminal SPARC fragment on TNBC cell adhesion, migration, transmigration and invasion

(A) Cell adhesion. MDA-MB-231 cells were let to adhere for 30 min on a fibronectin matrix in the presence of recombinant FL SPARC, recombinant cleaved SPARC fragments (cleaved SPARC), or purified 9-kDa C-terminal SPARC fragment at a final concentration of 240 nM. Left panels, representative images of adherent cells stained with crystal violet. Right panel, adhesion was quantified as described in Fig. 6A. Data are the mean ± SD (n=3); ***, $p<0.001$, ANOVA and Bonferroni's post hoc test. CTRL, PBS in cleavage buffer and SPARC-immunodepleted supernatant from the 9-kDa SPARC fragment purification. Similar results were obtained in three independent experiments.

(B) Cell migration. MDA-MB-231 cells were let to migrate for 16h on a fibronectin matrix in the absence or presence of FL SPARC, cleaved SPARC fragments, or the 9-kDa C-terminal SPARC fragment at a final concentration of 240 nM. Left panels, representative images of migrating cells stained with crystal violet. Right panel, migration was quantified as described in Fig. 6B. Data are the mean ± SD (n=3); ***, $p<0.001$, ANOVA and Bonferroni's post hoc test. CTRL, PBS in cleavage buffer and SPARC immunodepleted supernatant from the 9-kDa SPARC fragment purification. Similar results were obtained in two independent experiments.

(C) Endothelial transmigration. MDA-MB-231 cells were let to transmigrate for 16h through a HUVEC monolayer in the absence or presence of FL SPARC, cleaved SPARC fragments, or the 9-kDa C-terminal SPARC fragment at a final concentration of 240 nM. Left panels, representative images of transmigrating cells. Right panel, transmigrating cells were stained with MTT and quantified by absorbance at 570 nm. Data are the mean ± SD (n=3); *, $p<0.05$, **, $p<0.01$, ***, $p<0.001$, ANOVA and Bonferroni's post hoc test. CTRL, PBS in cleavage buffer and SPARC-immunodepleted supernatant from the 9-kDa SPARC fragment purification. Similar results were obtained in two independent experiments.

(D) Cell invasion. MDA-MB-231 cells were let to invade for 16h on a Matrigel matrix in the absence or presence of FL SPARC, cleaved SPARC fragments, or the 9-kDa C-terminal SPARC fragment at a final concentration of 240 nM. Left panels, representative images of invading cells stained with crystal violet. Right panel, invading cells were quantified by absorbance at 570 nm. Data are the mean ± SD (n=3); *, $p<0.05$, **, $p<0.01$, ***, $p<0.001$, ANOVA and Bonferroni's post hoc test. CTRL, PBS in cleavage buffer and SPARC immunodepleted supernatant from the 9-kDa SPARC fragment purification. Similar results were obtained in two independent experiments.

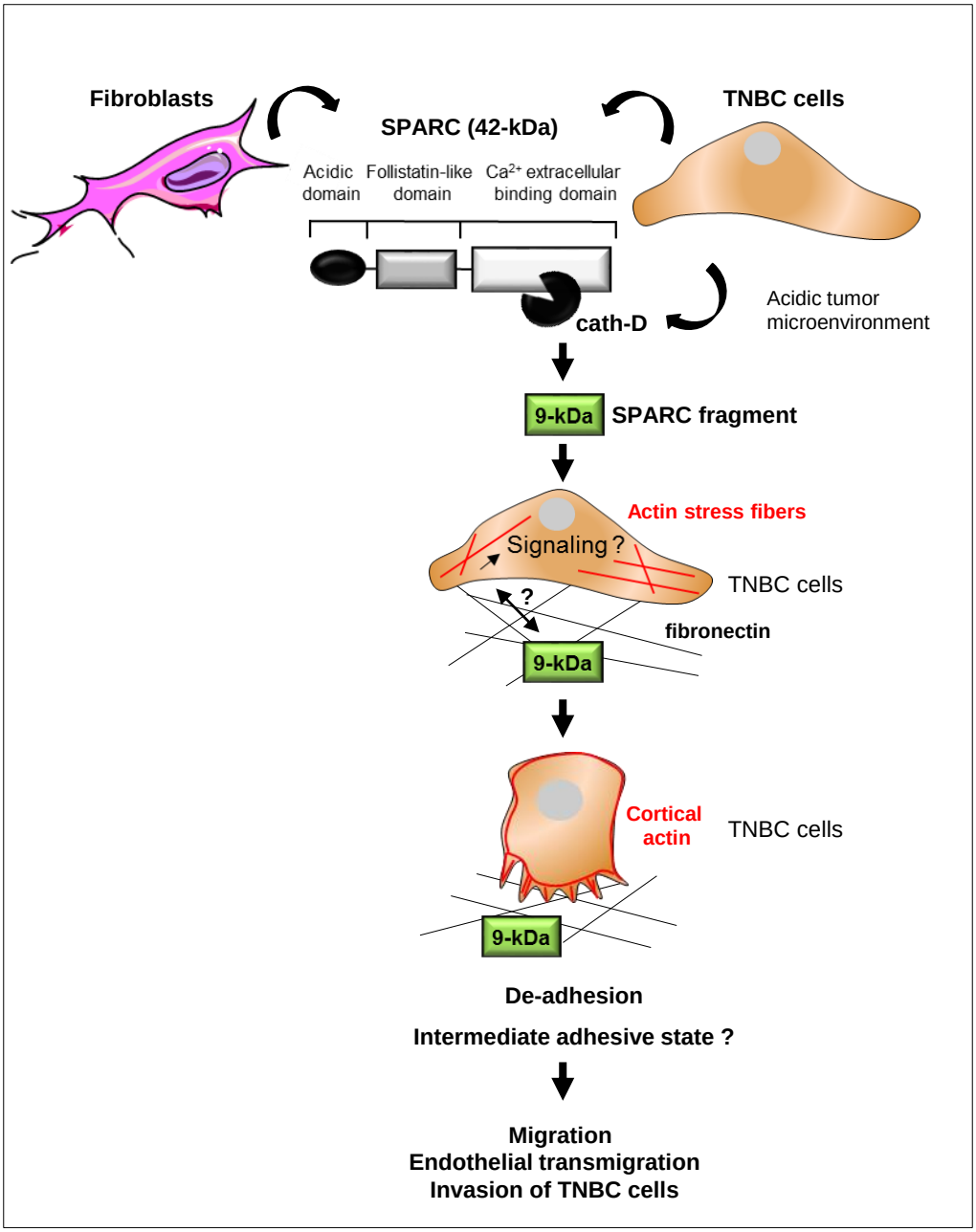

Fig. 9. Model of the 9-kDa C-terminal SPARC, released by cath-D cleavage, pro-tumor effect on TNBC cells TNBC-secreted cath-D triggers limited proteolysis of SPARC at the acidic pH of the tumor microenvironment

Among the SPARC fragments cleaved by cath-D, the 9-kDa C-terminal SPARC fragment inhibits TNBC cell adhesion and spreading. This might lead to an intermediate adhesive state, and stimulate TNBC cell migration, endothelial transmigration and invasion.

			ATOMS (*in vitro* cleavages of recombinant SPARC by recombinant cath-D)		TAILS (SPARC cleavages from conditioned media of cocultures)
SPARC peptides	SPARC fragments*	Enzyme used for sample digestion	(Pseudo-cathD + SPARC - pepst. /Pseudo-cath-D + SPARC +pepst) ratio (number of peptide identifications)	(Mature cath-D + SPARC -pepst. /Mature cath-D + SPARC + pepst.) ratio (number of peptide identifications)	(CM -pepst./CM +pepst.) ratio (number of peptide identifications)
LDSELTEFPLR [156-166]		Trypsin			0.4 (6)
DWLKNVLVTLYER [169-181]		Trypsin			0.5 (3)
VTLYERDEDNNLLTEK [176-191]	16-kDa	Trypsin	12.1 (5)	14.3 (5)	
YERDEDNNLLTEK [179-191]		Trypsin	13.7 (16)	11.8 (16)	
YERDEDNNLLTEKQK [179-193]		Trypsin	21.1 (15)	16.8 (15)	
EAGDHPVELLAR [207-218]	27-kDa	Trypsin	11.3 (6)	19.3 (6)	3.4 (2)
PVHWQFGQLDQHPIDGYLSHTELAPLR [230-256]	9-kDa	Trypsin			5.6 (8)
WQFGQLDQHPIDGYLSHTELAPLR [233-256]		Trypsin			3.1 (3)
FGQLDQHPIDGYLSHTELAPLR [235-256]		Trypsin	10.6 (5)	5.9 (5)	
GQLDQHPIDGYLSHTELAPLR [236-256]		Trypsin	2 (16)	2.3 (16)	12.4 (15)
QLDQHPIDGYLSHTELAPLR [237-256]		Trypsin	3.5 (5)	2.2 (5)	15.1 (5)
DQHPIDGYLSHTELAPLR [239-256]		Trypsin	8.4 (18)	8.1 (18)	7.6 (18)
YLSHTELAPLR [246-256]		Trypsin	18.8 (8)	5.7 (8)	4.4 (4)
LSHTELAPLR [247-256]		Trypsin			2.4 (1)
SHTELAPLR [248-256]		Trypsin	2.7 (5)	1.6 (5)	
PLIPMEHCTTR [258-268]	6- and 34-kDa	Trypsin	22.5 (15)	4.3 (15)	5.9 (3)
APQQEALPDE [18-27]		Glu-C		0.98 (2)	
APQQEALPDETE [18-29]		Glu-C		0.88 (13)	
APQQEALPDETEVVE [18-32]		Glu-C		1.12 (6)	
APQQEALPDETEVVEE [18-33]		Glu-C		1.1 (140)	
APQQEALPDETEVVEETVAE [18-37]		Glu-C		1.14 (18)	
VTLYERDEDNNLLTE [176-190]	16.4-kDa	Glu-C		**14.3** (12)	
YERDEDNNLLTE [179-190]		Glu-C		**13.1** (43)	
FGQLDQHPIDGYLSHTE [235-251]	9-kDa	Glu-C		**9.2** (3)	
GQLDQHPIDGYLSHTE [236-251]		Glu-C		**10.4** (12)	
DQHPIDGYLSHTE [239-251]		Glu-C		4.7 (6)	

Ratio ; <0.5 or >2 for trypsin ; Ratio ; <0.5 or >2 in bold for Glu-C; CM, conditioned medium ; pepst., pepstatin A ; *, according to silver staining.

Table 1. Sequences of the SPARC fragments identified by ATOMS and TAILS

High-confidence peptides with N-terminal iTRAQ labelling from the FL SPARC protein (Uniprot accession number P09486) identified by iTRAQ-ATOMS after *in vitro* cleavage of recombinant SPARC by recombinant cath-D, or by TAILS in the conditioned medium of co-cultured MDA-MB-231/HMFs. Peptides defining cleavage sites with iTRAQ ratios >2 or <0.5 for ATOMS or TAILS are shown. CM, conditioned medium; pepst., pepstatin A; *, according to the silver staining.